Title

Transcriptional Repression of *reaper* by Stand Still Safeguards Female Germline Development in *Drosophila*

Authors

Masaya Matsui[1], Shinichi Kawaguchi[1], and Toshie Kai[1,2]*

*Corresponding author

E-mail: kai.toshie.fbs@osaka-u.ac.jp (KT), kai.toshie.2w@kyoto-u.ac.jp (KT)

Affiliations

[1] Graduate School of Frontier Biosciences, The University of Osaka, Osaka 565-0871, Japan

[2] Graduate School of Biostudies, Kyoto University, Kyoto 606-8501, Japan

Abstract

Apoptosis plays a central role in shaping tissues and preserving cellular integrity across developmental stages. In the germline, its precise regulation is critical to ensure both the elimination of aberrant cells and the maintenance of reproductive capacity. However, the molecular mechanisms that control apoptotic susceptibility in germline cells remain poorly defined. Here, we identify *stand still* (*stil*) as a female germline-specific regulator of apoptosis in *Drosophila*. Loss of *stil* leads to near-complete depletion of germline cells at the time of eclosion, associated with upregulation of the pro-apoptotic gene *reaper* (*rpr*) and activation of caspase-dependent cell death. Reporter assays in S2 cells show that Stil directly represses *rpr* transcription through its N-terminal BED-type zinc finger domain. Despite the absence of *stil*, undifferentiated germline cells remain resistant to apoptosis. Analysis of publicly available chromatin data reveals that the *rpr* locus in these cells resides in a closed, H3K9me3-enriched chromatin state, suggesting a Stil-independent mode of transcriptional silencing. Together, our findings uncover two distinct mechanisms that protects the female germline from *rpr*-dependent apoptosis: Stil-mediated transcriptional repression that operates in both undifferentiated and differentiated germline cells, and an additional chromatin-based silencing mechanism that functions specifically in undifferentiated cells. This work provides new insights into the interplay between transcriptional and chromatin-based regulations that maintain germline cell identity and survival.

Introduction

Apoptosis, a form of programmed cell death (PCD), is a highly regulated biological process essential for animal development and tissue homeostasis. *Drosophila* is an excellent model organism for studying apoptotic cell death, due to its powerful genetic and molecular tools. In *Drosophila*, apoptosis is often initiated by the expression of IAP (inhibitor of apoptosis) antagonists, including members of the RHG gene family: *reaper* (*rpr*), *hid* (*head involution defective*), *grim*, and *sickle* (*skl*) (Abbott & Lengyel, 1991; P. Chen et al., 1996; Christich et al., 2002; White et al., 1994). Among these, the pro-apoptotic gene *rpr* plays a central role in PCD and stress-induced apoptosis (Yan et al., 2004). The *Drosophila* IAP protein DIAP1 is degraded via auto-ubiquitination, triggered by the physical interaction of Rpr through its conserved IAP-binding motif (IBM), leading to caspase activation and apoptotic cell death (Holley et al., 2002; Sandu et al., 2010). *rpr* expression is regulated by transcription factors and histone modifications, such as H3K27 and H3K9 trimethylation, in response to developmental and environmental signals (Beira et al., 2014; Brodsky et al., 2000; Jiang et al., 2000; Lohmann et al., 2002; Zhang et al., 2008).

For reproductive success, apoptosis is meticulously regulated to control cell numbers and maintain germline cell quality (Almeida et al., 2013; Chaudhry et al., 2021; Huang et al., 2023; Knudson et al., 1995). *Drosophila* adult female has a pair of ovaries, each containing 16–20 ovarioles. At the apical end of each ovariole lies the germarium, which houses germline stem cells (GSCs) that divide asymmetrically to produce a self-renewing GSC and a cystoblast. Cystoblast undergoes four mitotic divisions to form a 16-cell cyst

interconnected by ring canals. Of these 16 cells, one differentiates into the oocyte and enters meiosis, while the remaining 15 become nurse cells that support the oocyte by transporting proteins and RNAs. Encapsulated by somatic follicle cells, the cysts develop into egg chambers that progress through 14 stages, culminating in mature, fertilizable eggs (Gleason et al., 2018; Spradling et al., 2001).

To safeguard the fidelity of this process, apoptosis operates at two key checkpoints —within the germarium and during mid-oogenesis —ensuring that only healthy cells contribute to egg development. In the germarium, the first checkpoint triggers apoptotic cell death in response to DNA damage, mediated by p53-induced *hid* expression rather than *rpr* (Hou et al., 2008; Park et al., 2019). At the second checkpoint during mid-oogenesis, germline cells undergo caspase-regulated apoptotic and autophagic cell death in nutrient deprived condition, even though RHG genes are dispensable. (Baonza et al., 2022; Jeanne S. Peterson et al., 2007; T L Pritchett & McCall, 2012; Xing et al., 2015). Although apoptotic cell death is intricately regulated in response to various stimuli during oogenesis, the involvement of *rpr* in germline apoptosis remains largely unknown. Previous studies have identified *stand still* (*stil*) as a critical regulator of *Drosophila* germline cell survival (Schüpbach & Wieschaus, 1989). Genetic interactions with female germline-specific genes, such as *ovo* and *ovarian tumor* (*otu*), along with the female germline-specific requirement of *stil*, suggested its involvement in sex determination (G & D., 1997; Sahut-Barnola & Pauli, 1999). However, how Stil controls germline cell fate remains unknown. In this study, we identify *stil* as a repressor of *rpr* in female germline cells. Loss of *stil* function led to apoptosis-

89 mediated depletion of ovarian germline cells, associated with *rpr* upregulation.
90 Stil was enriched at the *rpr* locus and its upstream transcriptional control
91 region, suggesting a direct role in *rpr* regulation. Reporter assays in
92 *Drosophila* S2 cells revealed that Stil represses *rpr* transcription via its N-
93 terminal BED-type zinc finger domain, indicating its role as a repressive
94 transcription factor. In addition, we found that undifferentiated germline stem
95 cell (GSC)-like cells, in which the *rpr* locus exhibits a closed chromatin
96 structure, were resistant to apoptosis caused by *stil* loss. Our findings reveal a
97 molecular mechanism by which Stil and chromatin accessibility repress *rpr*,
98 providing novel insights into the regulation of germline cell fate.
99

100 **Results**

101 **Loss of *stand still* (*stil*) leads to female germline cell loss**

102 Previous studies have demonstrated the necessity of *standstill* (*stil*)
103 function in female germline cells; however, its molecular role remains elusive
104 (G & D., 1997; PK et al., 1996). To address this, we analyzed a loss of
105 function allele, $stil^{EY16156}$, which harbors a P-element insertion near the 3'end
106 of the second exon of *stil* gene, potentially disrupting the splicing of *stil*
107 transcripts (Fig 1A) (Bellen et al., 2004, 2011). RT-PCR revealed that *stil*
108 transcripts were undetectable in homozygous $stil^{EY16156}$ ovaries and in
109 $stil^{EY16156}$ testes, indicating a complete loss of *stil* expression in both gonads
110 (Fig. 1B).

111 Similar to the previously reported loss-of-function allele $stil^{3}$, which exhibited
112 the most severe phenotype (Fig. 1A; Fig. S1A, B) (PK et al., 1996), ovaries of
113 both $stil^{EY16156}$ homozygous and $stil^{EY16156}/Df(2R)vg\text{-}C$ trans-heterozygote, in
114 which the deficiency uncovers the entire *stil* locus, were severely reduced in
115 size and completely lacked germline cells (Fig. 1C, D). Likewise, $stil^{3}/stil^{EY16156}$
116 trans-heterozygote females exhibited more severe germline cell loss than
117 $stil^{3}/Df(2R)vg\text{-}C$ (Fig. S1A, B). However, male germline cell in $stil^{EY16156}$ testes
118 progressed to differentiate into mature sperms (Fig.S1A). Notably, fertility
119 assayed by egg production and hatching rate, was comparable between
120 $stil^{EY16156}$ and $stil^{EY16156}/CyO$ males (Fig. S1B), indicating that *stil* is specifically
121 required for female germline cells. The loss of germline cell in $stil^{EY16156}$
122 ovaries was fully rescued by overexpression of the *UASp-6×Myc-Stil*
123 transgene, driven by the germline-specific *NGT40; Nos-Gal4-VP16* driver
124 (Fig. 1C, D) (Grieder et al., 2000). Mutant females expressing 6×Myc-Stil,

125 germline cells were differentiated and developed into mature eggs that
126 hatched comparably to those of heterozygous control (Fig. 1E). Collectively,
127 these results confirm the pivotal role of *stil* in maintaining female germline
128 cells and ensuring proper oogenesis.
129
130 **_stil_-deficient germline cells undergo apoptotic cell death**
131 To investigate the cause of female germline cell loss, we knocked down *stil*
132 function by expressing short hairpin RNA targeting the 4th exon of the *stil*
133 transcript (GL01230) using a germline driver (Fig. 1A). Germline-specific
134 knockdown (*stil*-GLKD) reduced *stil* expression in ovaries by approximately
135 90% compared to control (Fig. 2A). *stil*-GLKD females contained significantly
136 smaller ovaries and did not lay any eggs, resembling to *stil* loss-of-function
137 mutant females (Fig. 2B and Fig. S2A). Unlike the complete germline loss
138 observed in *stil* mutants, however, most ovarioles in *stil*-GLKD retained
139 germline cells, indicating a milder phenotype (Fig. 2C). Notably, the number of
140 ovarioles containing at least two egg chambers was remarkably fewer (27.4%
141 versus 100% in the control), suggesting that oogenesis was perturbed before
142 mid-oogenesis (Fig. 2B, D). While *stil*-GLKD exhibited severe defects similar
143 to its loss-of function alleles, its somatic knockdown using a tj-Gal4 driver (*stil*-
144 STKD) did not affect egg production and the hatching rate at all (Fig. S2A).
145 These observations suggest that *stil* functions in germline cells both for the
146 survival of female germline cells and egg development.
147 Previous studies have suggested that stil may play a role in sex
148 determination, particularly through its genetic interaction with *ovo* and the key
149 sex determination regulator *otu*, which represses the male identity factor

150 Tdrd5l (G & D., 1997; Primus et al., 2019; Sahut-Barnola & Pauli, 1999) . To
151 investigate whether *stil* is involved in sex determination, we examined the
152 transcripts of *sxl*, a master regulator of sex determination of germline cells in
153 *stil* mutant ovaries (Hashiyama et al., 2011). *sxl* pre-mRNA undergoes
154 alternative splicing to generate sex-specific isoforms, producing a functional
155 Sxl protein essential for female development, or a truncated non-functional
156 male-specific isoform (Bell et al., 1991) (Moschall et al., 2019). RT-PCR
157 revealed an enrichment of the female-specific *sxl* isoform in both control and
158 *stil*-GLKD ovaries (Fig. S2B). In addition, male-specific *sxl* transcripts,
159 detected in both control and *stil*-GLKD testes, were absent in *stil*-GLKD
160 ovaries, indicating that *sxl* splicing patterns remain unaffected by *stil*
161 depletion. These results suggest that *stil* functions independently of sex
162 identity determination in germline cells.
163 Damaged or abnormal cells are typically removed through regulated cell
164 death mechanisms, including apoptosis, autophagy, and necrosis (Fuchs &
165 Steller, 2011, 2015). In *Drosophila* ovaries, such cell death occurs at two
166 distinct developmental checkpoints during oogenesis: in the germarium and
167 during mid-oogenesis, in response to either developmental cues or
168 environmental stressors (McCall, 2004; Tracy L. Pritchett et al., 2009). To
169 determine whether germline cell loss in *stil*-deficient ovaries was due to
170 apoptosis, we performed a TUNEL (Terminal deoxynucleotidyl Transferase
171 Biotin dUTP Nick End Labeling) assay, which detects DNA fragmentation
172 indicative of apoptotic cell death. In region 2A and 2B of the germarium, the
173 first developmental checkpoint in oogenesis (Drummond-Barbosa &
174 Spradling, 2001), the number of TUNEL-positive cells significantly increased

175 in *stil*-GLKD ovaries compared to controls (Fig. 2E, F). These results suggest
176 that *stil*-GLKD germline cells undergoes apoptotic cell death.
177 To further confirm the involvement of *stil* in apoptosis, we overexpressed
178 inhibitor of apoptosis proteins (IAPs) in *stil* mutant germline cells. Both the
179 *Drosophila* protein DIAP1 (Death-associated inhibitor of apoptosis 1) and the
180 baculovirus-derived P35 are well-characterized inhibitors that can effectively
181 suppress apoptosis in *Drosophila*. DIAP1 inhibits the activity of initiator
182 caspase, Dronc (Death regulator Nedd2-like caspase) which activates effector
183 caspase, while P35 directly inhibits effector caspase (Baum et al., 2007; J.S
184 Peterson et al., 2003; Werz et al., 2005). Germline-specific overexpression of
185 P35 fully rescued the germline cell loss observed in $stil^{EY16156}$ mutants (Fig.
186 2G, H). However, germline development remained arrested, and egg
187 chambers degenerated at the mid-oogenesis (Fig. S3). Likewise, DIAP1
188 overexpression partially restored germline cells (~50% of ovarioles retained
189 germline cells), but did not fully rescue oogenesis defects (Fig. 2G, H).
190 Altogether, these findings indicate that the loss of *stil* function not only triggers
191 apoptosis that can be suppressed by apoptosis inhibitors but also causes
192 defects in oogenesis progression that are not rescued by blocking cell death.
193

194 **Stil regulates proapoptotic genes to suppress apoptosis in female**
195 **germline cells**

196 Stil protein harbors a characteristic DNA-binding domain, BED-type zinc
197 finger, containing highly conserved aromatic residues followed by a shared
198 pattern of cysteines and histidines (Fig. S4A) (Aravind, 2000). Given that
199 many of the known BED-type zinc fingers including the founder members,

200 BEAF and DREF, function as transcription factors or chromatin regulators
201 (McKowen et al., 2022; Sokolova et al., 2023; Tue et al., 2017), Stil may play
202 a role in transcriptional regulation. To examine this possibility, we analyzed
203 the transcriptional profiles of ovarian RNA of *stil* mutant and control. We took
204 advantage of the ectopic expression of P35 to overcome cell death defect of
205 germline cells due to the loss of in *stil* function. The RNA-seq analysis
206 identified 3,569 (30.7%) differentially expressed genes (DEGs) (log2FC>|1|
207 and p-adj<0.01) out of 11,608 annotated genes (PRJDB20709;
208 Supplementary Table 1). Among these, 2,044 genes were up-regulated
209 (17.6 %, red dots) and 1,525 genes were down-regulated (13.1 %, blue dots)
210 in *stil* mutant ovaries (Fig. S4B). Consistent with the observation of
211 developmental arrest and egg chambers degeneration at the mid-stage of
212 oogenesis (Fig. S3), genes known to be highly expressed in late-stage
213 oogenesis, such as proteins composing the chorion, were significantly
214 downregulated in *stil* mutant ovaries (Fig. 3A). Of those upregulated, notably,
215 the proapoptotic gene *rpr* (*reaper*) ranked among the top 10 upregulated
216 DEGs (Fig. 3A). Given the apoptotic phenotype of *stil* mutant germline cells,
217 67 apoptosis-related genes out of 224 annotated in the dataset (GO:0006915)
218 were identified as DEGs (Fig. 3B). Among the top 10 genes list of apoptosis-
219 related DEGs, proapoptotic genes, *rpr* and *hid* (*head involution defective*),
220 were significantly upregulated, while the hedgehog signaling genes expressed
221 in later oogenesis such as *ptc*, *duox*, and *rdx* were significantly downregulated
222 (Fig. 3C). *rpr* and *hid* are the key members of IAP antagonists, known for their
223 central role in initiating apoptosis (Abbott & Lengyel, 1991; White et al., 1994).
224 Their activation through various signaling pathways leads to the ubiquitin-

225 mediated degradation and translational inhibition of DIAP1, which
226 subsequently results in the activation of Caspase proteins (Freel et al., 2008;
227 Holley et al., 2002). Further validation by RT-qPCR demonstrated that *rpr*
228 expression increased approximately 700-fold, while *hid* expression increased
229 15-fold in the rescued *stil* mutant ovaries by P35 expression (Fig. 3D). To
230 exclude a possibility that egg chamber degeneration in germline-rescued *stil*
231 mutants affects proapoptotic gene expression, we isolated RNAs from early-
232 stage ovaries (up to stage 5-6 of oogenesis) by manual removal of later
233 stages and re-examined their expression levels. *rpr* expression remained
234 elevated in RNAs prepared from early-stage ovaries, while *hid* expression did
235 not (Fig. S4B). Furthermore, RT-qPCR analysis using *stil*-GLKD ovaries
236 driven by three different germline drivers, *NGT40*; *NosGal4-VP16*, *Bam-Gal4*,
237 and *mat*α *-Tub-Gal4*, consistently exhibited significant upregulation of *rpr* but
238 not *hid* across all conditions (Fig. S5A). Conversely, *rpr* was not prominently
239 upregulated in *stil*-GLKD testes with *NGT40*; *NosGal4-VP16* or *Bam-Gal4*,
240 consistent with the phenotypic observations in *stil* mutant testes (Fig. S5C).
241 These results suggest that *rpr* is robustly upregulated in the absence of *stil*
242 function in female germline cells.
243 To determine whether proapoptotic genes upregulation directly contributes to
244 apoptosis of *stil* mutant female germline cells, we generated double mutants
245 of *stil* and the proapoptotic gene, *rpr*. Strikingly, the germline cell death and
246 differentiation defects observed in *stil* mutant ovaries were fully rescued in the
247 double mutant ovaries (Fig. 3E, F). Germline development proceeded,
248 resulting in the formation of mature eggs and partial restoration of fertility;
249 mutant females laid a few eggs and approximately 40 % of those hatched

250 (Fig. 3G, H). In contrast, *stil-hid* double mutants showed a slight increase in
251 germline cell survival, but no developing egg chambers were observed (Fig.
252 S5D, E), indicating that *hid* does not play a central role in apoptosis caused by
253 the loss of *stil* function. These findings highlight that *rpr* regulation by *stil* is
254 critical for suppressing apoptosis in female germline cells, establishing *rpr* as
255 a key downstream effector in this pathway.
256

257 **Stil represses *rpr* expression by targeting the regulatory regions via its**
258 **BED-type zinc finger**

259 The transcription of *rpr* is governed by a complex network of
260 developmental, environmental, and stress-related signals, each employing
261 distinct regulatory mechanisms. These signals modulate transcription factors
262 such as p53, Dfd, the EcR/USP complex, AP-1, Shn, leading to either the
263 activation or suppression of apoptosis (Beira et al., 2014; Brodsky et al., 2000;
264 Jiang et al., 2000; Lohmann et al., 2002). These transcription factors interact
265 with upstream enhancer and promoter regions of the *rpr* locus (*rpr*-
266 transcriptional control region) to either activate or suppress its transcription,
267 ensuring precise spatial and temporal control of apoptosis (Fuchs & Steller,
268 2011). To examine whether Stil also directly interacts with *rpr*-transcriptional
269 control region, we performed DNA adenine methyltransferase identification
270 (DamID)-seq analysis (Aughey et al., 2019). A fusion of Stil with *E. coli* DNA
271 adenine methyltransferase (Dam-Stil) or Dam alone as a control were
272 expressed specifically in germline cells (Díaz-Torres et al., 2021; Southall et
273 al., 2013). Genomic DNA from ovaries was digested with DpnI and subjected
274 to NGS to detect GATC sites methylated by Dam-Stil near Stil-bound regions

275 (PRJDB20722). Genome-wide DamID-seq analysis revealed that ~80% of
276 Stil-enriched peaks were located in promoter regions, supporting a role for Stil
277 in transcriptional regulation (Fig. 4A). At higher resolution, prominent peaks
278 were observed at the *rpr* locus and its upstream region (5–6 kb), suggesting
279 direct binding of Stil to the *rpr* regulatory element (Fig. 4B).Next, we examined
280 the role of Stil's BED-type zinc finger in *rpr* repression by generating four Stil
281 variants: Stil-FL (full-length), Stil-NT (N-terminal domain containing the BED-
282 type zinc finger and nuclear localization signal), Stil-CT (C-terminal domain
283 lacking these two motifs), and Stil-AAYA (full-length Stil with a mutated BED-
284 type zinc finger substituting four residues including two critical cysteines) (Fig.
285 4C). In nurse cells, despite lacking the predicted nuclear localization signal,
286 Stil-CT localized to the nucleus and overlapped with chromosomes, as did
287 Stil-FL and Stil-AAYA, whereas Stil-NT showed diffuse nuclear distribution
288 without being enriched onto chromosomes (Fig. S6A). Collectively, these data
289 suggest that Stil's nuclear and chromatin localization are mediated by the C-
290 terminal domain, independently of the zinc finger motif. To assess the
291 functional significance of these domains *in vivo*, we expressed the variants in
292 *stil*^{EY16156} germline cells. Stil-FL fully rescued the defects of both germline cell
293 survival and development, leading to the production of mature eggs (Fig. 4D,
294 E, F). Remarkably, Stil-NT partially rescued germline defects despite its
295 diffuse nuclear localization, while neither Stil-CT nor Stil-AAYA, both lacking
296 functional BED-type zinc fingers, restored germline cell survival or
297 differentiation. These findings suggest that the BED-type zinc finger is
298 essential for Stil function in germline cells possibly as a transcription regulator,
299 while the C-terminal domain mediates nuclear and chromatin localization.

300 To validate whether the BED-type zinc finger functions in *rpr* repression
301 through interaction with the *rpr* transcriptional control region, we performed a
302 reporter assay using *Drosophila* S2 cells. We constructed a *rpr*-GFP reporter
303 containing the 5-kb upstream region of *rpr*, where DamID-seq signals were
304 detected, fused to GFP (Fig. 4G) and transfected with Still variants. Stil
305 variants exhibited localization patterns in S2 cells similar to those in nurse
306 cells (Fig. S6B), supporting their suitability for functional analysis in S2 cells.
307 Consistent with the *in vivo* rescue experiment (Fig.4 D-F), co-expression of
308 Stil-FL with the *rpr*-GFP reporter significantly repressed GFP expression. Stil-
309 NT containing the BED-type zinc finger also reduced GFP expression, albeit
310 partially. In contrast, Stil-CT and Stil-AAYA failed to exhibit any detectable
311 repressive effects (Fig. 4H). To confirm the specificity of this Stil-mediated
312 repression, we utilized a *ubiP*-GFP reporter containing the *ubi-p63E* gene
313 promoter fused to GFP (Fig. S6C). Co-expression of Stil-FL with the *ubiP*-
314 GFP reporter showed no reduction in GFP expression (Fig. S6D), suggesting
315 that Stil preferentially targets the *rpr* upstream region. These results
316 demonstrate that Stil interacts with the *rpr* transcriptional control region via its
317 BED-type zinc finger, which is critical for transcriptional repression, while the
318 chromatin association through the C-terminal region is required for full
319 repressive activity in germline cells.
320

321 **Undifferentiated Germline Cells Exhibit Resistance to Apoptosis in *stil***
322 **loss**

323 Loss of *stil* function resulted in severe depletion of germline cells by the 3rd
324 instar larval stage (120 hours after egg laying, AEL), leaving only a few

325 surviving germline cells in *stil* mutant (Fig. 5A, B). Notably, these surviving
326 germline cells were predominantly found near the terminal filaments and
327 future cap cells, the niche that supports germline stem cell (GSC) (Fig.
328 5A)(Spradling et al., 2001). This observation suggested that GSCs within the
329 niche may be resistant to cell death caused by *stil* loss. To test whether GSCs
330 are inherently resistant to cell death caused by *stil* deficiency, we induced
331 GSC-like properties by overexpressing a constitutively active the
332 Decapentaplegic (Dpp) receptor, Thickveins (Tkv.CA) in germline cells, or the
333 loss of function of *bag of marbles* (*bam*), a key differentiation factor
334 (Casanueva & Ferguson, 2004; D. Chen & McKearin, 2003a). These
335 manipulations resulted in the tumorigenic proliferation of undifferentiated
336 GSC-like cells or pre-cystoblast, respectively (Tiwari et al., 2019).
337 Remarkably, Tkv.CA overexpression and *bam* loss rescued germline cell
338 depletion in *stil* mutant ovaries, leading to the formation of tumorous germaria
339 containing undifferentiated germline cells comparable to the *stil* heterozygous
340 control (Fig. 5C, D). Indeed, TUNEL assay showed no increase in apoptotic
341 cells in such tumorous germaria (Fig. 5E, F), indicating that the
342 undifferentiated state of germline cells confers resistance to apoptosis in the
343 absence of *stil*.
344 Consistent with this observation, RNA-seq and gene Ontology (GO)
345 analysis of those tumorous ovaries revealed that the expression levels of
346 most apoptosis-related genes (GO:0006915), including *rpr*, remain unaffected
347 (PRJDB20709; Supplementary Table 2) (Fig. 5G). Furthermore, RT-qPCR
348 confirmed that *rpr* expression was not significantly upregulated in the GSC-
349 like tumor *stil* mutant ovaries compared to p35-rescued *stil* mutant ones (Fig.

350 3D, 5H), suggesting that apoptosis-related genes, including *rpr*, are
351 transcriptionally repressed in GSC-like cells even in the absence of *stil*
352 function.
353

354 **_rpr_ Silencing in Undifferentiated Germline Cells Is Associated with**
355 **Chromatin States**

356 Previous studies in mammals have established that stem cells are
357 generally resistant to apoptosis. In mouse mammary stem cells and cancer
358 stem cells, this resistance is attributed to several mechanisms, including
359 enhanced DNA repair and overexpression of anti-apoptotic proteins (Chang et
360 al., 2015; Nathansen et al., 2021; Safa, 2016). Similarly, in *Drosophila*,
361 intestinal stem cells were shown to resist cell death through a two-tiered
362 regulation of *rpr*, involving chromatin state and spatial control of its expression
363 (Sulekh et al., 2024). To explore whether chromatin dynamics contribute to
364 GSC apoptosis resistance in *stil* mutants, we analyzed the chromatin status at
365 the *rpr* locus using Assay for Transposase-Accessible Chromatin-seq (ATAC-
366 seq) data of *Drosophila* ovarian cells (Pang et al., 2023). This dataset was
367 generated using fluorescence-activated cell sorting (FACS) of GSCs (2C–4C)
368 and nurse cells (NCs) at various stages of egg chamber maturation, with
369 ploidy levels ranging from 4C to 512C due to endoreplication (Dej &
370 Spradling, 1999). In early mid-stage NCs where *stil* deficient-germline cells
371 undergo apoptosis, ATAC-seq signals were enriched at three upstream
372 regions of *rpr* (-0.5 to 0.5 kb, 1.5 to 2.0 kb, and 3.5 to 5.0 kb relative to the
373 transcription start site [TSS] of *rpr*) (Fig. 6A). Conversely, signals at these
374 three regions were significantly lower in 2C-4C GSCs and 64C-512C NCs.

375 These results suggest that the chromatin state upstream of *rpr* is closed in
376 GSCs and late-stage NCs (64C-512C) but open in early mid-stage NCs (4C-
377 32C). Notably, despite harboring the same ploidy, 4C GSCs and 4C NCs
378 displayed distinct chromatin accessibility, reflecting regulatory differences
379 likely responsible for their differential responses to apoptosis (Fig. 6A). We
380 further analyzed epigenetic marks such as H3K9me3 and H3K27me3 at the
381 *rpr* locus using publicly available data sets (DeLuca et al., 2020; Pang et al.,
382 2023). H3K9me3, a histone modification associated with transcriptional
383 repression, was observed around the *rpr* locus and its transcriptional control
384 region in GSCs, whereas only minimal signals were detected in 4C NCs (Fig.
385 6B). In contrast, H3K27me3, another repression mark exhibited no difference
386 between GSC and st5 NC (Fig. 6C) (DeLuca et al., 2020). This suggests that
387 H3K9me3, rather than H3K27me3, may establish a heterochromatic state at
388 the *rpr* loci in GSCs, contributing to transcriptional silencing. These findings
389 imply that chromatin dynamics play a crucial role in regulating *rpr* expression
390 during germline development.

391 **Discussion**

392 In this study, we investigated the role of the *Drosophila* gene *stand still* (*stil*),
393 which is required for the survival and maturation of female germline cells.
394 Loss of *stil* leads to apoptosis of germline cells via upregulation of the pro-
395 apoptotic gene *rpr* (Fig. 3E), identifying *rpr* as the primary effector of cell
396 death in this context. GFP-reporter assays with Stil variants in S2 cells
397 suggest that Stil represses *rpr* expression, likely through direct binding to its
398 upstream regulatory region via the BED-type zinc finger domain (Fig. 4H).

399 The transcription of *rpr* is regulated by multiple transcription factors
400 that bind to cis-regulatory elements located upstream of the gene (Fuchs &
401 Steller, 2011). For example, the tumor suppressor protein p53 binds to a well-
402 characterized p53 response element (p53RE) located 4.8 kb upstream of *rpr*,
403 which is responsive to intrinsic and extrinsic signals during embryogenesis
404 and in germline cells (Lu et al., 2010; Wylie et al., 2014). However, p53
405 binding to this element has only been observed in the anterior germarium, and
406 no direct link between p53 and apoptosis has been established in the female
407 germline (Park et al., 2019). Other known regulators, such as the homeobox
408 transcription factor Deformed (Dfd) and the JNK-responsive complex AP-1,
409 also bind upstream *rpr* enhancers in somatic tissues, but neither is active in
410 the female germline (Beira et al., 2014; Lohmann et al., 2002). Thus, factors
411 that suppress *rpr* transcription specifically in germline cells have remained
412 unidentified. Our study identifies Stil as a female germline-specific repressor

413 of *rpr*. DamID profiling revealed Stil binding to the *rpr* locus to 5–6 kb
414 upstream, covering regulatory elements associated with known transcription
415 factors (Fig. 4B). Consistently, Stil repressed *rpr*-GFP reporter containing the
416 5 kb upstream regulatory region in S2 cells, and this repression required Stil's
417 BED-type zinc finger domain (Fig. 4H). This domain is known to mediate DNA
418 binding and contribute to transcriptional regulation and chromatin remodeling
419 (Aravind, 2000). These findings support a model in which Stil directly occupies
420 the *rpr* regulatory region and blocks activator access to maintain
421 transcriptional repression in germline cells.

422 Whereas DIAP1 overexpression only partially rescued germline loss
423 in *stil* mutants, P35 restored germline survival in nearly all cases (Fig. 2G, H),
424 highlighting a functional distinction in how these inhibitors act in the context of
425 *rpr*-induced apoptosis. Both inhibit apoptosis through distinct mechanisms:
426 DIAP1 blocks caspase activation by inhibiting initiator and effector caspases,
427 while P35, a baculoviral protein, acts as a pseudo-substrate that irreversibly
428 inhibits effector caspases such as DrICE and Dcp-1 (Li et al., 2024; Nair &
429 Baker, 2024). *rpr* antagonizes DIAP1 through two independent mechanisms—
430 by promoting its auto-ubiquitination and proteasomal degradation, and by
431 inhibiting its translation (Freel et al., 2008; Holley et al., 2002). Therefore, high
432 *rpr* levels in *stil* mutant ovaries may deplete functional DIAP1, limiting the
433 rescue effect of its overexpression. By contrast, P35 directly targets
434 downstream caspases, bypassing DIAP1 loss and producing stronger

435 inhibition. These results support the model that Stil maintains the apoptotic
436 threshold by regulating *rpr* levels and balancing Rpr–DIAP1 interactions
437 (Sandu et al., 2010; Yin & Thummel, 2004).

438 Despite the loss of *stil*, undifferentiated female germline cells (GSCs
439 and pre-cyst cells) remain resistant to apoptosis (Fig. 5E, F), correlating with
440 closed chromatin and H3K9me3 enrichment at the *rpr* locus (Fig. 6A, B).
441 Similar chromatin-based repression of *rpr* has been reported in *Drosophila*
442 intestinal stem cells (Sulekh et al., 2024) and in late-stage embryos, where
443 heterochromatin silences *rpr* expression (Zhang et al., 2008). Together with
444 our findings, these studies suggest that chromatin-mediated silencing
445 provides an additional layer of protection against apoptosis in female GSCs,
446 independent of *stil*. By contrast, *stil* mutant male germline cells show no
447 phenotype and no *rpr* upregulation (Fig. S5B), suggesting that that *rpr*-
448 mediated apoptosis is not activated in the male germline. This points to a sex-
449 specific mechanism of *rpr* repression, potentially involving chromatin-based
450 silencing, although this possibility has yet to be examined.

451 Together, our findings reveal two mechanisms that protect female
452 germline cells from *rpr*-dependent apoptosis: Stil-mediated transcriptional
453 repression, which operates in both differentiated and undifferentiated germline
454 cells, and chromatin-based silencing, which functions specifically in
455 undifferentiated germline cells (Fig. 6D). Although the upstream regulation of

456 *stil* is unknown, its selective role in female germline cells suggests it functions
457 as a developmental checkpoint that prevents premature apoptosis during
458 oogenesis. A key question is how *stil* integrates intrinsic or environmental
459 cues to modulate the apoptotic threshold during germline development.
460

461 ## Materials and Methods

462 ### Fly stock and cultures

463 All *Drosophila* stocks and crosses were reared at room temperature (25ºC) on
464 standard food [5% (w/v) dry yeast, 5% (w/v) corn flower, 2% (w/v) rice bran,
465 10% (w/v) glucose, 0.7% (w/v) agar, 0.2% (v/v) propionic acid and 0.05%
466 (w/v) p-hydroxy butyl benzoic acid]. The following stocks were used in this
467 study: *yellow white* (*y w)*, *attP2* (BL#25710), $stil^{EY16156}$ (BL#21191), $stil^{3}$
468 (BL#533, splicing donor site of the second intron was mutated from GTATG to
469 ATATG at 12570993), *Df(2R)vg-C* (BL#754, deficiency for *stil*), *Df(3L)X14*
470 (BL#600368, deficiency for *hid*) *UASp-P35* (a gift from Dr. Bergmann), *UASp-*
471 *DIAP1* (BL#63818), rpr^{87} (BL#83150), hid^{05014} (BL#83349), *UASp-Tkv.CA* (a
472 gift from Dr. Dahua Chen), $bam^{\Delta 86}$ (BL#5427), *NGT40-Gal4*; *nosGal4-VP16*
473 (Grieder et al., 2000), *mat* α*-tub-Gal4* (BL#7063), *bam-Gal4* (D. Chen &
474 McKearin, 2003b) , and *tj-Gal4* (DGRC#104055). The mutation site of $stil^{3}$
475 was identified by sanger sequencing of the PCR-amplified fragment.

476

477 ### Generation of transgenic fly lines

478 Transgenic fly lines expressing Stil variants (6×Myc-Stil-FL, 6×Myc-Stil-NT,
479 6×Myc-Stil-CT, and 6×Myc-Stil-AAYA) and DamID constructs (Dam-alone and
480 Dam-Stil) were generated using the PhiC31 integrase-mediated transgenesis
481 system. DNA fragments encoding Stil variant were amplified using cDNAs
482 obtained by reverse transcription of ovarian RNA extracted from *y w* flies.

483 DamID constructs were designed such that a primary open reading frame
484 (ORF) encoding GFP was followed by two stop codons and a secondary ORF
485 encoding either Dam or Dam-Stil (Southall et al., 2013). The DNA fragment
486 encoding Dam was amplified from the pUASTattB-LT3-NDam vector (a gift
487 from Dr. Andrea H. Brand). The resulting DNA fragments were cloned into the
488 pUASp-K10-attB plasmid backbone (Koch et al., 2009). These transgenic
489 constructs were injected into embryos of attP-containing strains (Stil variants
490 into P40, BDSC #25709, Dam and Dam-Stil into P2, BDSC #25710,
491 respectively), and transformants expressing *mini-white* were selected.

492

493 **Immunofluorescence staining**

494 Immunofluorescence staining was performed as previously described (Xu et
495 al., 2024). Ovaries and testis from adults and the 3rd instar larva were
496 dissected in cold phosphate buffer saline (PBS) and fixed with PBS containing
497 5.3% (w/v) paraformaldehyde for 10 min. Fixed samples were washed in PBX
498 [PBS with 0.2% (v/v) Triton-X (Nacalai)] for at least 30 min with several
499 change of solution, then blocked with PBX containing 4% (w/v) bovine serum
500 albumin (BSA) for at least 30 min at room temperature. After rinsing once with
501 PBX, the samples were incubated with the primary antibodies diluted in PBX
502 containing 0.4% (w/v) BSA for more than 4 h at room temperature or
503 overnight at 4ºC. After several washes with PBX for at least 1 h, the samples
504 were incubated in secondary antibodies diluted in PBX containing 0.4% (w/v)

505 BSA for more than 2 h at room temperature. The samples were washed
506 several times with PBX for at least 1 h and stained with 1 μg/ml of 4',6-
507 diamidino-2phenylindole (DAPI) (Sigma) diluted in PBX for 10 min at room
508 temperature. Following two rinses with PBX and PBS, tissues were mounted
509 in Fluoro-KEEPER Antifade Reagent (Nacalai). The following primary
510 antibodies were used at the indicated dilutions: guinea pig anti-Vas (1:1000)
511 (Patil & Kai, 2010), mouse anti c-Myc [Wako (9E10), 1:500], and rabbit anti-
512 FLAG [MBL, PM020, 1:1000]. Secondary antibodies were Alexa Fluor 488-
513 and 555-conjugated goat antibodies against rabbit, mouse and guinea pig IgG
514 (Invitrogen, A11029, A11034, A11073, A21424, A21429 and A21435) at a
515 1:200 dilution in PBX containing 0.4% (w/v) BSA. Images were captured by
516 Zeiss LSM780 Confocal Microscope with 10x, 20x, and 40x lens and
517 processed with Zen (Zeiss) and Fiji application (Schindelin et al., 2012) .

518

519 **TUNEL assay**

520 TUNEL assay was conducted using ApopTag® Kits (Millipore), labelling the
521 free 3'-OH DNA termini in situ with fluorescein-nucleotide by terminal
522 deoxynucleotidyl transferase (TdT). Dissected ovaries in cold PBS were fixed
523 with PBS containing 5.3% (w/v) paraformaldehyde and rinsed 3 times with
524 PBX. Ovaries were washed with PBX for 10 min twice and further washed
525 with PBST [PBS with 0.1% (v/v) Tween 20 (Nacalai)] twice. After rinsing with
526 Equilibration Buffer twice, the samples were incubated with TdT reagent [70%

527 (v/v) Reaction Buffer and 30% (v/v) TdT Enzyme] for 1 h at 37ºC. After
528 incubation with 1/35 diluted Stop/Wash Buffer for 15 min, samples were
529 rinsed 3 times with PBX and then washed 3 times with PBX for 10 min. The
530 tissue mounting and microscopic observation were as described in the
531 "Immunofluorescence staining" section.

532

533 **RT-PCR and quantitative RT-PCR**

534 Total RNA was isolated from ovaries using TRIzol LS Reagent (Invitrogen),
535 following the manufacturer's protocol. RNA samples (1 µg each) were treated
536 with DNase I (NEB) to digest genomic DNA, followed by inactivation of the
537 enzyme with 5 mM EDTA at 75ºC for 10 min. Reverse transcription was
538 performed using the DNase I-treated RNA with oligo(dT)20 primers and
539 SuperScript III Reverse Transcriptase (Invitrogen), following the
540 manufacturer's protocol. cDNAs were subjected to 30 cycles of RT-PCR with
541 GoTaq DNA polymerase (Promega).

542 Quantitative PCR (qPCR) was performed with Fast SYBR Green regents
543 (Invitrogen) using at least 3 biological replicates. Deltal-delta-CT method was
544 used to obtain the relative transcript levels. *α-Tub84B (tubulin)* was used as
545 the reference. The sequences of the primers are listed in Supplementary
546 Table 3.

547

548 **mRNA-seq analysis**

549 Total RNAs were extracted from 100 ovaries of control and *stil* mutant of
550 *Tkv.CA OE* background and 40 ovaries of control and *stil* mutant of *P35 OE*
551 background using TRIzol (ThermoFisher) following the manufacture's
552 instruction. Extracted RNAs were treated with DNase I for 10 min at 37ºC and
553 reactions were inhibited by 5 mM EDTA at 70ºC for 10 min, following that
554 RNAs were purified using phenol/ chloroform/ isoamyl alcohol (mixed with a
555 ratio of 25: 24: 1, pH 5.2). Purified RNAs were prepared for mRNA-seq
556 libraries with NEBNext Ultra II RNA Library Prep Kit for Illumina (NEB), and
557 deep-sequencing was conducted using NovaSeq6000 (Illumina). Sequencing
558 analysis was conducted using bioinformatic software, CLC workbench 12
559 (QIAGEN). Adaptor sequences of total reads obtained from mRNA-seq were
560 trimmed and reads were mapped to *Drosophila* genomes, r6.32 from Flybase
561 (ftp://ftp.flybase.net/genomes/Drosophila_melanogaster/). After mapping the
562 sequence data, Differential expression analysis was performed between
563 control and *stil* mutant with *P35 OE* or*Tkv.CA OE* and calculated the
564 expression level of each gene.

565

566 **DamID-seq and data processing**

567 UASp-Dam and UASp-Dam-Stil flies were crossed with *NGT40; NosGal4-*
568 *VP16* driver and maintained at 25°C. For each replicate, 100 ovaries of 50
569 flies were dissected in *Drosophila* Schneider's medium. Genomic DNA was
570 extracted using the QIAamp Fast DNA Tissue Kit (QIAGEN cat. no. 51404),
571 and methylated DNA was processed and amplified as described (Díaz-Torres
572 et al., 2021). Briefly, genomic DNA was digested overnight with *Dpn*I (NEB),
573 which cuts methylated GATC sites, and DamID adaptors were ligated to the
574 resulting fragments. A subsequent digestion with *Dpn*II (NEB), which
575 selectively cuts unmethylated GATC sites, was performed, and fragments
576 containing consecutive methylated GATCs were then amplified by PCR using
577 ligated adaptor-specific primers and PrimeSTAR® HS DNA Polymerase
578 (Takara).

579 The amplified DNA was sonicated using a Bioruptor (Diagenode) to obtain an
580 average fragment size of 300 bp. DamID adaptors were removed by digestion
581 with *Alw*I, and the DNA was purified using AMPure XP beads (Beckman
582 Coulter). For next-generation sequencing, the DNA was subjected to end-
583 repair, A-tailing, Illumina adaptor ligation, and PCR amplification. Single-end
584 100 bp reads were subsequently generated on a NovaSeq 6000 platform
585 (Illumina). Illumina NGS reads were aligned to the *Drosophila melanogaster*
586 reference genome (r6.32), and enrichment profiles were generated using the
587 damidseq_pipeline with default settings (Marshall & Brand, 2015), with
588 replicate libraries subsequently averaged. The Dam-Stil enrichment profile

589 was normalized by the Dam control profile and Dam-Stil peaks were identified
590 using find_peaks and annotated with the ChIPseeker pipeline (Marshall &
591 Brand, 2015) .

592

593 **Fertility test**

594 For female fertility assays, three virgin females were mated with three *y w*
595 males for 3 days per replicate. For male fertility assays, three males were
596 mated with three *y w* virgin females under the same conditions. After the
597 mating period, eggs were collected for 24 hours, followed by incubation for an
598 additional 24 hours. The total number of eggs and the number of hatched
599 eggs were then counted for each replicate.

600

601 **S2 cell culture experiments**

602 *Drosophila* Schneider S2 cells were cultured at 28°C in Schneider's medium
603 (Thermo) supplemented with 10% (v/v) fetal bovine serum (FBS), 100 U/mL
604 penicillin, and 100 µg/mL streptomycin (Thermo). Plasmids encoding Stil
605 variants were generated using the Gateway cloning system with (Life
606 Technologies) with pAFW, which drives the expression of N-terminal FLAG-
607 tagged fusion proteins under the control of the Actin5C promoter. *rpr*-GFP and

608 *ubiP*-GFP reporter plasmid was constructed by replacing 2.4-kb tubulin
609 promoter of the *tubP*-GFP, a gift from Dr, Steve Cohen (Brennecke et al.,
610 2003), with the PCR-amplified 5-kb promoter region and 5'-UTR of *rpr* and the
611 PCR-amplified 2,137 bp promoter region and 5'-UTR of *ubi-p63E*.

612 For the reporter assay, a total of 4 μg of plasmid DNA was used for each
613 transfection. Transgenes and reporter plasmids were included at 1 μg each as
614 needed, and the remaining amount was supplemented with the control
615 plasmid pAW without attR sites to reach 4 μg. The plasmid mixture was
616 combined with 20 μL of Hilymax transfection reagent (Dojindo) and
617 transfected into 1 mL of S2 cells seeded one day prior, following the
618 manufacturer's instructions. Two days of post-transfection, cells were
619 collected, sonicated, and followed by centrifugation. The supernatant was
620 mixed with 20% volume of 5× sample buffer. Proteins were then analyzed by
621 Western blotting using the following antibodies and Signal Enhancer Reagent
622 HIKARI (Nacalai): mouse anti-α-Tubulin [Santa Cruz, DM1A, 1:1000] rabbit
623 anti-GFP [Clonetech, 632569, 1:1000], and rabbit anti-FLAG [MBL, PM020,
624 1:1000]. Chemiluminescence detection was performed using the Chemi-Lumi
625 One reagent kit (Nacalai), and immunoreactive bands were visualized with a
626 ChemiDoc Touch imaging system (Bio-Rad) and analyzed using Fiji
627 (Schindelin et al., 2012).

628 For immunostaining, transfected S2 cells were collected at 2-days post-
629 transfection and plated onto poly-L-Lysine-coated coverslips for at least 30
630 min to promote adhesion. Cells were fixed in 5.3% (w/v) paraformaldehyde for
631 15 min, permeabilized with PBX for 10 min, and washed three times with
632 PBX. After blocking with PBX containing 4% (w/v) BSA for 30 min, cells were
633 incubated with primary and secondary antibodies for at least 1 hour each,
634 followed by nuclear staining with 1 μg/ml of DAPI for 10 min. After rinsing with
635 PBS, samples were mounted with Fluoro-KEEPER Antifade Reagent
636 (Nacalai). Images were acquired using a Zeiss LSM780 and 900 confocal
637 microscopes with a 63× objective lens and processed using Zen and ImageJ
638 software.

639

Competing Interest Statement

The authors declare that the research was conducted in the absence of any commercial or financial relationships that could be construed as a potential conflict of interest.

Acknowledgments

We thank Dr. Andrea H. Brand (The Gurdon Institute, University of Cambridge), Dr. Andreas Bergmann (UMass Chan Medical School, Massachusetts), and Dr. Dahua Chen (Yunnan University Institute of Biomedical Research, Kunming) for their generous gifts of the Dam CDS plasmid, the UASp-P35 transgenic fly line, and the UASp-Tkv.CA transgenic fly line, respectively. We acknowledge Bloomington Drosophila Stock Centre for the fly stocks. Confocal images and Western blotting data were acquired with LSM780, LSM900 and ChemiDoc Touch, respectively, at FBS Core Facility in The University of Osaka. We appreciate the insightful discussion and suggestions from all the members of KT's laboratory.

Author Contributions

All authors contributed to the experiment design. MM, KS, and KT performed all experiments. MM and KS performed the computational analyses. MM, KS, and KT wrote the paper. KS and KT supervised the project.

662 ## References

663 Abbott, M. K. & Lengyel, J. A. (1991). Embryonic head involution and rotation
664 of male terminalia require the Drosophila locus head involution defective.
665 *Genetics*, *129*(3), 783–789. https://doi.org/10.1093/genetics/129.3.783

666 Almeida, C., Correia, S., Rocha, E., Alves, Â., Ferraz, L., Silva, J., Sousa, M.
667 & Barros, A. (2013). Caspase signalling pathways in human
668 spermatogenesis. *Journal of Assisted Reproduction and Genetics*, *30*(4),
669 487–495. https://doi.org/10.1007/s10815-013-9938-8

670 Aravind, L. (2000). The BED finger, a novel DNA-binding domain in
671 chromatin-boundary-element-binding proteins and transposases. *Trends in*
672 *Biochemical Sciences*, *25*(9), 421–423. https://doi.org/10.1016/s0968-
673 0004(00)01620-0

674 Aughey, G. N., Cheetham, S. W. & Southall, T. D. (2019). DamID as a
675 versatile tool for understanding gene regulation. *Development*, *146*(6),
676 dev173666. https://doi.org/10.1242/dev.173666

677 Baonza, A., Tur-Gracia, S., Pérez-Aguilera, M. & Estella, C. (2022).
678 Regulation and coordination of the different DNA damage responses in
679 Drosophila. *Frontiers in Cell and Developmental Biology*, *10*, 993257.
680 https://doi.org/10.3389/fcell.2022.993257

681 Baum, J. S., Arama, E., Steller, H. & McCall, K. (2007). The Drosophila
682 caspases Strica and Dronc function redundantly in programmed cell death
683 during oogenesis. *Cell Death & Differentiation*, *14*(8), 1508–1517.
684 https://doi.org/10.1038/sj.cdd.4402155

685 Beira, J. V., Springhorn, A., Gunther, S., Hufnagel, L., Pyrowolakis, G. &
686 Vincent, J.-P. (2014). The Dpp/TGFβ-Dependent Corepressor Schnurri
687 Protects Epithelial Cells from JNK-Induced Apoptosis in Drosophila
688 Embryos. *Developmental Cell*, *31*(2), 240–247.
689 https://doi.org/10.1016/j.devcel.2014.08.015

690 Bell, L. R., Horabin, J. I., Schedl, P. & Cline, T. W. (1991). Positive
691 autoregulation of Sex-lethal by alternative splicing maintains the female
692 determined state in Drosophila. *Cell*, *65*(2), 229–239.
693 https://doi.org/10.1016/0092-8674(91)90157-t

694 Bellen, H. J., Levis, R. W., He, Y., Carlson, J. W., Evans-Holm, M., Bae, E.,
695 Kim, J., Metaxakis, A., Savakis, C., Schulze, K. L., Hoskins, R. A. &
696 Spradling, A. C. (2011). The Drosophila Gene Disruption Project: Progress

697 Using Transposons With Distinctive Site Specificities. *Genetics*, *188*(3),
698 731–743. https://doi.org/10.1534/genetics.111.126995

699 Bellen, H. J., Levis, R. W., Liao, G., He, Y., Carlson, J. W., Tsang, G., Evans-
700 Holm, M., Hiesinger, P. R., Schulze, K. L., Rubin, G. M., Hoskins, R. A. &
701 Spradling, A. C. (2004). The BDGP Gene Disruption Project. *Genetics*,
702 *167*(2), 761–781. https://doi.org/10.1534/genetics.104.026427

703 Brennecke, J., Hipfner, D. R., Stark, A., Russell, R. B. & Cohen, S. M. (2003).
704 bantam Encodes a Developmentally Regulated microRNA that Controls
705 Cell Proliferation and Regulates the Proapoptotic Gene hid in Drosophila.
706 *Cell*, *113*(1), 25–36. https://doi.org/10.1016/s0092-8674(03)00231-9

707 Brodsky, M. H., Nordstrom, W., Tsang, G., Kwan, E., Rubin, G. M. & Abrams,
708 J. M. (2000). Drosophila p53 Binds a Damage Response Element at the
709 reaper Locus. *Cell*, *101*(1), 103–113. https://doi.org/10.1016/s0092-
710 8674(00)80627-3

711 Casanueva, M. O. & Ferguson, E. L. (2004). Germline stem cell number in the
712 Drosophila ovary is regulated by redundant mechanisms that control Dpp
713 signaling. *Development*, *131*(9), 1881–1890.
714 https://doi.org/10.1242/dev.01076

715 Chang, C.-H., Zhang, M., Rajapakshe, K., Coarfa, C., Edwards, D., Huang, S.
716 & Rosen, J. M. (2015). Mammary Stem Cells and Tumor-Initiating Cells Are
717 More Resistant to Apoptosis and Exhibit Increased DNA Repair Activity in
718 Response to DNA Damage. *Stem Cell Reports*, *5*(3), 378–391.
719 https://doi.org/10.1016/j.stemcr.2015.07.009

720 Chaudhry, S. R., Lopes, J., Levin, N. K., Kalpage, H. & Tainsky, M. A. (2021).
721 Germline mutations in apoptosis pathway genes in ovarian cancer; the
722 functional role of a TP53I3 (PIG3) variant in ROS production and DNA
723 repair. *Cell Death Discovery*, *7*(1), 62. https://doi.org/10.1038/s41420-021-
724 00442-y

725 Chen, D. & McKearin, D. (2003a). Dpp Signaling Silences bam Transcription
726 Directly to Establish Asymmetric Divisions of Germline Stem Cells. *Current*
727 *Biology*, *13*(20), 1786–1791. https://doi.org/10.1016/j.cub.2003.09.033

728 Chen, D. & McKearin, D. M. (2003b). A discrete transcriptional silencer in the
729 bam gene determines asymmetric division of the Drosophila germline stem
730 cell. *Development*, *130*(6), 1159–1170. https://doi.org/10.1242/dev.00325

731 Chen, P., Nordstrom, W., Gish, B. & Abrams, J. M. (1996). grim, a novel cell
732 death gene in Drosophila. *Current Biology*, *6*(7), 767.
733 https://doi.org/10.1016/s0960-9822(02)00588-2

734 Christich, A., Kauppila, S., Chen, P., Sogame, N., Ho, S.-I. & Abrams, J. M.
735 (2002). The Damage-Responsive Drosophila Gene sickle Encodes a Novel
736 IAP Binding Protein Similar to but Distinct from reaper, grim, and hid.
737 *Current Biology*, *12*(2), 137–140. https://doi.org/10.1016/s0960-
738 9822(01)00658-3

739 Dej, K. J. & Spradling, A. C. (1999). The endocycle controls nurse cell
740 polytene chromosome structure during Drosophila oogenesis.
741 *Development*, *126*(2), 293–303. https://doi.org/10.1242/dev.126.2.293

742 DeLuca, S. Z., Ghildiyal, M., Pang, L.-Y. & Spradling, A. C. (2020).
743 Differentiating Drosophila female germ cells initiate Polycomb silencing by
744 regulating PRC2-interacting proteins. *ELife*, *9*, e56922.
745 https://doi.org/10.7554/elife.56922

746 Díaz-Torres, A., Rosales-Nieves, A. E., Pearson, J. R., Mateos, C. S.-C.,
747 Marín-Menguiano, M., Marshall, O. J., Brand, A. H. & González-Reyes, A.
748 (2021). Stem cell niche organization in the Drosophila ovary requires the
749 ECM component Perlecan. *Current Biology*, *31*(8), 1744-1753.e5.
750 https://doi.org/10.1016/j.cub.2021.01.071

751 Drummond-Barbosa, D. & Spradling, A. C. (2001). Stem Cells and Their
752 Progeny Respond to Nutritional Changes during Drosophila Oogenesis.
753 *Developmental Biology*, *231*(1), 265–278.
754 https://doi.org/10.1006/dbio.2000.0135

755 Freel, C. D., Richardson, D. A., Thomenius, M. J., Gan, E. C., Horn, S. R.,
756 Olson, M. R. & Kornbluth, S. (2008). Mitochondrial Localization of Reaper
757 to Promote Inhibitors of Apoptosis Protein Degradation Conferred by GH3
758 Domain-Lipid Interactions*. *Journal of Biological Chemistry*, *283*(1), 367–
759 379. https://doi.org/10.1074/jbc.m708931200

760 Fuchs, Y. & Steller, H. (2011). Programmed Cell Death in Animal
761 Development and Disease. *Cell*, *147*(4), 742–758.
762 https://doi.org/10.1016/j.cell.2011.10.033

763 Fuchs, Y. & Steller, H. (2015). Live to die another way: modes of programmed
764 cell death and the signals emanating from dying cells. *Nature Reviews*
765 *Molecular Cell Biology*, *16*(6), 329–344. https://doi.org/10.1038/nrm3999

766 G, P. & D., P. (1997). stand still, a Drosophila gene involved in the female
767 germline for proper survival, sex determination and differentiation.
768 *Genetics*, *145*(4), 975–987. https://doi.org/10.1093/genetics/145.4.975

769 Gleason, R. J., Anand, A., Kai, T. & Chen, X. (2018). Protecting and
770 Diversifying the Germline. *Genetics*, *208*(2), 435–471.
771 https://doi.org/10.1534/genetics.117.300208

772 Grieder, N. C., Cuevas, M. de & Spradling, A. C. (2000). The fusome
773 organizes the microtubule network during oocyte differentiation in
774 Drosophila. *Development*, *127*(19), 4253–4264.
775 https://doi.org/10.1242/dev.127.19.4253

776 Hashiyama, K., Hayashi, Y. & Kobayashi, S. (2011). Drosophila Sex lethal
777 Gene Initiates Female Development in Germline Progenitors. *Science*,
778 *333*(6044), 885–888. https://doi.org/10.1126/science.1208146

779 Holley, C. L., Olson, M. R., Colón-Ramos, D. A. & Kornbluth, S. (2002).
780 Reaper eliminates IAP proteins through stimulated IAP degradation and
781 generalized translational inhibition. *Nature Cell Biology*, *4*(6), 439–444.
782 https://doi.org/10.1038/ncb798

783 Hou, Y.-C. C., Chittaranjan, S., Barbosa, S. G., McCall, K. & Gorski, S. M.
784 (2008). Effector caspase Dcp-1 and IAP protein Bruce regulate starvation-
785 induced autophagy during Drosophila melanogaster oogenesis. *The*
786 *Journal of Cell Biology*, *182*(6), 1127–1139.
787 https://doi.org/10.1083/jcb.200712091

788 Huang, C., Zhao, S., Yang, Y., Guo, T., Ke, H., Mi, X., Qin, Y., Chen, Z.-J. &
789 Zhao, S. (2023). TP63 gain-of-function mutations cause premature ovarian
790 insufficiency by inducing oocyte apoptosis. *Journal of Clinical Investigation*,
791 *133*(5), e162315. https://doi.org/10.1172/jci162315

792 Jiang, C., Lamblin, A.-F. J., Steller, H. & Thummel, C. S. (2000). A Steroid-
793 Triggered Transcriptional Hierarchy Controls Salivary Gland Cell Death
794 during Drosophila Metamorphosis. *Molecular Cell*, *5*(3), 445–455.
795 https://doi.org/10.1016/s1097-2765(00)80439-6

796 Knudson, C. M., Tung, K. S. K., Tourtellotte, W. G., Brown, G. A. J. &
797 Korsmeyer, S. J. (1995). Bax-Deficient Mice with Lymphoid Hyperplasia
798 and Male Germ Cell Death. *Science*, *270*(5233), 96–99.
799 https://doi.org/10.1126/science.270.5233.96

800 Koch, R., Ledermann, R., Urwyler, O., Heller, M. & Suter, B. (2009).
801 Systematic Functional Analysis of Bicaudal-D Serine Phosphorylation and

802 Intragenic Suppression of a Female Sterile Allele of BicD. *PLoS ONE*, *4*(2),
803 e4552. https://doi.org/10.1371/journal.pone.0004552

804 Li, J., Jordana, L., Mehsen, H., Wang, X. & Archambault, V. (2024). Nuclear
805 reassembly defects after mitosis trigger apoptotic and p53-dependent
806 safeguard mechanisms in Drosophila. *PLOS Biology*, *22*(8), e3002780.
807 https://doi.org/10.1371/journal.pbio.3002780

808 Lohmann, I., McGinnis, N., Bodmer, M. & McGinnis, W. (2002). The
809 Drosophila Hox Gene Deformed Sculpts Head Morphology via Direct
810 Regulation of the Apoptosis Activator reaper. *Cell*, *110*(4), 457–466.
811 https://doi.org/10.1016/s0092-8674(02)00871-1

812 Lu, W.-J., Chapo, J., Roig, I. & Abrams, J. M. (2010). Meiotic Recombination
813 Provokes Functional Activation of the p53 Regulatory Network. *Science*,
814 *328*(5983), 1278–1281. https://doi.org/10.1126/science.1185640

815 Marshall, O. J. & Brand, A. H. (2015). damidseq_pipeline: an automated
816 pipeline for processing DamID sequencing datasets. *Bioinformatics*,
817 *31*(20), 3371–3373. https://doi.org/10.1093/bioinformatics/btv386

818 McCall, K. (2004). Eggs over easy: cell death in the Drosophila ovary.
819 *Developmental Biology*, *274*(1), 3–14.
820 https://doi.org/10.1016/j.ydbio.2004.07.017

821 McKowen, J. K., Avva, S. V. S. P., Maharjan, M., Duarte, F. M., Tome, J. M.,
822 Judd, J., Wood, J. L., Negedu, S., Dong, Y., Lis, J. T. & Hart, C. M. (2022).
823 The Drosophila BEAF insulator protein interacts with the polybromo subunit
824 of the PBAP chromatin remodeling complex. *G3*, *12*(11), jkac223.
825 https://doi.org/10.1093/g3journal/jkac223

826 Moschall, R., Rass, M., Rossbach, O., Lehmann, G., Kullmann, L., Eichner,
827 N., Strauss, D., Meister, G., Schneuwly, S., Krahn, M. P. & Medenbach, J.
828 (2019). Drosophila Sister-of-Sex-lethal reinforces a male-specific gene
829 expression pattern by controlling Sex-lethal alternative splicing. *Nucleic*
830 *Acids Research*, *47*(5), 2276–2288. https://doi.org/10.1093/nar/gky1284

831 Nair, S. & Baker, N. E. (2024). Extramacrochaetae regulates Notch signaling
832 in the Drosophila eye through non-apoptotic caspase activity. *ELife*, *12*,
833 RP91988. https://doi.org/10.7554/elife.91988

834 Nathansen, J., Meyer, F., Müller, L., Schmitz, M., Borgmann, K. & Dubrovska,
835 A. (2021). Beyond the Double-Strand Breaks: The Role of DNA Repair
836 Proteins in Cancer Stem-Cell Regulation. *Cancers*, *13*(19), 4818.
837 https://doi.org/10.3390/cancers13194818

838 Pang, L.-Y., DeLuca, S., Zhu, H., Urban, J. M. & Spradling, A. C. (2023).
839 Chromatin and gene expression changes during female Drosophila
840 germline stem cell development illuminate the biology of highly potent stem
841 cells. *ELife*, *12*(6), RP90509. https://doi.org/10.7554/elife.90509

842 Park, J.-H., Nguyen, T. T. N., Lee, E.-M., Castro-Aceituno, V., Wagle, R., Lee,
843 K.-S., Choi, J. & Song, Y.-H. (2019). Role of p53 isoforms in the DNA
844 damage response during Drosophila oogenesis. *Scientific Reports*, *9*(1),
845 11473. https://doi.org/10.1038/s41598-019-47913-y

846 Patil, V. S. & Kai, T. (2010). Repression of Retroelements in Drosophila
847 Germline via piRNA Pathway by the Tudor Domain Protein Tejas. *Current*
848 *Biology*, *20*(8), 724–730. https://doi.org/10.1016/j.cub.2010.02.046

849 Peterson, Jeanne S., Bass, B. P., Jue, D., Rodriguez, A., Abrams, J. M. &
850 McCall, K. (2007). Noncanonical cell death pathways act during Drosophila
851 oogenesis. *Genesis*, *45*(6), 396–404. https://doi.org/10.1002/dvg.20306

852 Peterson, J.S, Barkett, M. & McCall, K. (2003). Stage-specific regulation of
853 caspase activity in drosophila oogenesis. *Developmental Biology*, *260*(1),
854 113–123. https://doi.org/10.1016/s0012-1606(03)00240-9

855 PK, M., AR, C. & JR, J. (1996). Mutations in the gene stand still disrupt germ
856 cell differentiation in Drosophila ovaries. *Developmental Genetics*, *18*(4),
857 316–324. https://doi.org/10.1002/(sici)1520-6408(1996)18:4<316::aid-
858 dvg5>3.0.co;2-c

859 Primus, S., Pozmanter, C., Baxter, K. & Doren, M. V. (2019). Tudor-domain
860 containing protein 5-like promotes male sexual identity in the Drosophila
861 germline and is repressed in females by Sex lethal. *PLoS Genetics*, *15*(7),
862 e1007617. https://doi.org/10.1371/journal.pgen.1007617

863 Pritchett, T L & McCall, K. (2012). Role of the insulin/Tor signaling network in
864 starvation-induced programmed cell death in Drosophila oogenesis. *Cell*
865 *Death & Differentiation*, *19*(6), 1069–1079.
866 https://doi.org/10.1038/cdd.2011.200

867 Pritchett, Tracy L., Tanner, E. A. & McCall, K. (2009). Cracking open cell
868 death in the Drosophila ovary. *Apoptosis*, *14*(8), 969.
869 https://doi.org/10.1007/s10495-009-0369-z

870 Safa, A. R. (2016). Resistance to Cell Death and Its Modulation in Cancer
871 Stem Cells. *Critical Reviews in Oncogenesis*, *21*(3–4), 203–219.
872 https://doi.org/10.1615/critrevoncog.2016016976

873 Sahut-Barnola, I. & Pauli, D. (1999). The Drosophila gene stand still encodes
874 a germline chromatin-associated protein that controls the transcription of
875 the ovarian tumor gene. *Development*, *126*(9), 1917–1926.
876 https://doi.org/10.1242/dev.126.9.1917

877 Sandu, C., Ryoo, H. D. & Steller, H. (2010). Drosophila IAP antagonists form
878 multimeric complexes to promote cell death. *Journal of Cell Biology*,
879 *190*(6), 1039–1052. https://doi.org/10.1083/jcb.201004086

880 Schindelin, J., Arganda-Carreras, I., Frise, E., Kaynig, V., Longair, M.,
881 Pietzsch, T., Preibisch, S., Rueden, C., Saalfeld, S., Schmid, B., Tinevez,
882 J.-Y., White, D. J., Hartenstein, V., Eliceiri, K., Tomancak, P. & Cardona, A.
883 (2012). Fiji: an open-source platform for biological-image analysis. *Nature*
884 *Methods*, *9*(7), 676–682. https://doi.org/10.1038/nmeth.2019

885 Schüpbach, T. & Wieschaus, E. (1989). Female sterile mutations on the
886 second chromosome of Drosophila melanogaster. I. Maternal effect
887 mutations. *Genetics*, *121*(1), 101–117.
888 https://doi.org/10.1093/genetics/121.1.101

889 Sokolova, O., Morgunova, V., Sizova, T. V., Komarov, P. A., Olenkina, O. M.,
890 Babaev, D. S., Mikhaleva, E. A., Kwon, D. A., Erokhin, M. & Kalmykova, A.
891 (2023). The insulator BEAF32 controls the spatial-temporal expression
892 profile of the telomeric retrotransposon TART in the Drosophila germline.
893 *Development*, *150*(12). https://doi.org/10.1242/dev.201678

894 Southall, T. D., Gold, K. S., Egger, B., Davidson, C. M., Caygill, E. E.,
895 Marshall, O. J. & Brand, A. H. (2013). Cell-Type-Specific Profiling of Gene
896 Expression and Chromatin Binding without Cell Isolation: Assaying RNA
897 Pol II Occupancy in Neural Stem Cells. *Developmental Cell*, *26*(1), 101–
898 112. https://doi.org/10.1016/j.devcel.2013.05.020

899 Spradling, A., Drummond-Barbosa, D. & Kai, T. (2001). Stem cells find their
900 niche. *Nature*, *414*(6859), 98–104. https://doi.org/10.1038/35102160

901 Sulekh, S., Ikegawa, Y., Naito, S., Oji, A., Hiratani, I. & Yoo, S. K. (2024). A
902 feedback loop that drives cell death and proliferation and its defect in
903 intestinal stem cells. *Life Science Alliance*, *7*(4), e202302238.
904 https://doi.org/10.26508/lsa.202302238

905 Tiwari, M. D., Zeitler, D. M., Meister, G. & Wodarz, A. (2019). Molecular
906 profiling of stem cell-like female germ line cells in Drosophila delineates
907 networks important for stemness and differentiation. *Biology Open*, *8*(11),
908 bio046789. https://doi.org/10.1242/bio.046789

909 Tue, N. T., Yoshioka, Y., Mizoguchi, M., Yoshida, H., Zurita, M. & Yamaguchi,
910 M. (2017). DREF plays multiple roles during Drosophila development.
911 *Biochimica et Biophysica Acta (BBA) - Gene Regulatory Mechanisms*,
912 *1860*(6), 705–712. https://doi.org/10.1016/j.bbagrm.2017.03.004

913 Werz, C., Lee, T. V., Lee, P. L., Lackey, M., Bolduc, C., Stein, D. S. &
914 Bergmann, A. (2005). Mis-specified cells die by an active gene-directed
915 process, and inhibition of this death results in cell fate transformation in
916 Drosophila. *Development*, *132*(24), 5343–5352.
917 https://doi.org/10.1242/dev.02150

918 White, K., Grether, M. E., Abrams, J. M., Young, L., Farrell, K. & Steller, H.
919 (1994). Genetic Control of Programmed Cell Death in Drosophila. *Science*,
920 *264*(5159), 677–683. https://doi.org/10.1126/science.8171319

921 Wylie, A., Lu, W.-J., D'Brot, A., Buszczak, M. & Abrams, J. M. (2014). p53
922 activity is selectively licensed in the Drosophila stem cell compartment.
923 *ELife*, *3*, e01530. https://doi.org/10.7554/elife.01530

924 Xing, Y., Su, T. T. & Ruohola-Baker, H. (2015). Tie-mediated signal from
925 apoptotic cells protects stem cells in Drosophila melanogaster. *Nature*
926 *Communications*, *6*(1), 7058. https://doi.org/10.1038/ncomms8058

927 Xu, F., Suyama, R., Inada, T., Kawaguchi, S. & Kai, T. (2024). HemK2
928 functions for sufficient protein synthesis and RNA stability through eRF1
929 methylation during Drosophila oogenesis. *Development*, *151*(14).
930 https://doi.org/10.1242/dev.202795

931 Yan, N., Wu, J.-W., Chai, J., Li, W. & Shi, Y. (2004). Molecular mechanisms of
932 DrICE inhibition by DIAP1 and removal of inhibition by Reaper, Hid and
933 Grim. *Nature Structural & Molecular Biology*, *11*(5), 420–428.
934 https://doi.org/10.1038/nsmb764

935 Yin, V. P. & Thummel, C. S. (2004). A balance between the diap1 death
936 inhibitor and reaper and hid death inducers controls steroid-triggered cell
937 death in Drosophila. *Proceedings of the National Academy of Sciences*,
938 *101*(21), 8022–8027. https://doi.org/10.1073/pnas.0402647101

939 Zhang, Y., Lin, N., Carroll, P. M., Chan, G., Guan, B., Xiao, H., Yao, B., Wu,
940 S. S. & Zhou, L. (2008). Epigenetic Blocking of an Enhancer Region
941 Controls Irradiation-Induced Proapoptotic Gene Expression in Drosophila
942 Embryos. *Developmental Cell*, *14*(4), 481–493.
943 https://doi.org/10.1016/j.devcel.2008.01.018

944

945 ## Legends

946 **Figure 1. Disruption of *stil* induces female germline cell depletion**

947 (A) Schematic representation of the *Drosophila stil* gene locus showing the
948 position of P-element insertion, *EY16156*, mutation site of $stil^3$, and the target
949 site of shRNA for knockdown. Black and blue arrows represent primers for RT-
950 PCR and RT-qPCR, respectively. (B) Expression of *stil* and the control *α-tub*
951 transcripts in $stil^{EY16156}$ mutant and the heterozygous control ovaries or testes
952 analyzed by RT-PCR. (C) Representative images showing entire ovarian
953 morphology (left panels) and ovarioles immunostained with with a germline
954 marker, Vasa (red), and nuclear staining with DAPI (blue) (right panels) from *y*
955 *w*, $stil^{EY16156}/CyO$, $stil^{EY16156}$, $stil^{EY16156}/Df$, and $stil^{EY16156}$ expressing *6×Myc-Stil-*
956 *FL* transgene driven by the germline-specific driver, *NGT40; NosGal4-VP16*.
957 Scale bar: 1 mm for whole ovaries in the left panels, 50 μm for ovariole in the
958 right panels. (D) Quantification of the percentage of germline cell-containing
959 ovarioles in 2-3-days old females. Genotypes are indicated below the graph
960 and the numbers of ovarioles assessed are shown above each bar. Error bars
961 represent standard deviation (s.d.). (E) Analysis of egg laying and hatching rate.
962 The egg numbers and their hatching rate by three females indicated genotypes
963 corresponding to those in (C) mated with three *y w* males were measured daily
964 (n=3). Error bars indicate s.d.

965

966 **Figure 2. *stil* loss induces apoptotic cell death in female germline cells**

967 (A) Quantitative RT-PCR confirming the knockdown efficiency in ovaries of *stil*-
968 germline knockdown (*stil*-GLKD) where shRNA targeting stil transcript was
969 driven by *NGT40; NosGal4-VP16*, and the control with shRNA alone.
970 Expression levels of an internal control, *rp49*, and *stil* are normalized to that of
971 *α-tub*. Error bar indicates s.d. (*n*=3). (B) Representative images showing entire
972 ovarian morphology (left panels) and ovarioles immunostained with a germline
973 marker, Vasa (red), and nuclear staining with DAPI (blue) (right panels) from
974 *stil*-GLKD and the control with shRNA alone. Scale bar: 1 mm for whole ovaries
975 and 50 μm for ovarioles, respectively. (C) Quantification of the percentage of
976 germline cell-containing ovarioles in 2-3-days old females. Genotypes are
977 indicated below the graph and the number of germarium assessed is noted
978 above each bar. Error bars represent standard deviation (s.d.). (D)
979 Quantification of the percentage of developed ovarioles defined as ovarioles
980 that contain at least two egg chambers beyond the germarium. Genotypes are
981 indicated below the graph and the number of germarium assessed is noted
982 above each bar. Error bars represent standard deviation (s.d.). (E)
983 Representative images of TUNEL-positive apoptotic cells (green), Vasa (red),
984 and DAPI (blue) in control with shRNA alone and *stil*-GLKD germaria (white
985 dotted). Scale bar: 20 μm. (F) Quantification of apoptosis in germarium with
986 TUNEL assay in control and *stil*-GLKD. (G) Representative images of germaria
987 (white dotted) from $stil^{EY16156}$, $stil^{EY16156}$*; P35 OE* (*NGT40; NosGal4-VP16> P35*),

988 and *stil*^{EY16156}; *DIAP1 OE* (*NGT40; NosGal4-VP16> DIAP1*) immunostained
989 with Vasa (red) with DAPI (blue). Scale bar: 20 μm. (H) Quantification of the
990 percentage of germline cell-containing ovarioles in 2–3-day old females.
991 Genotypes are indicated below the graph and the number of germarium
992 assessed is noted above each bar. Error bars indicate standard deviation (s.d.).

993

994 **Figure 3. *stil* regulates *rpr* expression in female germline cells**

995 (A) Top 10 upregulated and downregulated genes in *stil*-deficient ovaries. Bars
996 indicate fold changes in *stil* mutant ovaries overexpressing (OE) of the
997 apoptosis inhibitor, P35 in germline cells (*stil*^{EY16156}*, NGT40; NosGal4-VP16>*
998 *P35*), compared to control with P35 OE in a heterozygous background
999 (*stil*^{EY16156}*/CyO, NGT40; NosGal4-VP16> P35*). Bars are according to adjusted
1000 p-values (p-adj). (B) MA plot of apoptosis-related genes (GO:0006915) showing
1001 their mean gene expression (CPM: counts per million) and fold change in
1002 *stil*^{EY16156}*; P35 OE* comparing *stil*^{EY16156}*/CyO; P35 OE*. Each dot represents an
1003 individual gene, with dot size inversely correlated with p-value adjusted (p-adj).
1004 Larger dots highlight genes with higher statistical significance. The red dots
1005 (upregulated genes) and blue dots (downregulated genes) represent the
1006 differentially expressed RNAs with fold threshold>2.0, and p-adj<0.01. (C) Top
1007 10 upregulated and downregulated genes related to apoptosis (GO:0006915).
1008 Bars represent fold changes and are colored by adjusted p-values (p-adj), as

1009 in (A). (D) Quantitative RT-PCR analysis of proapoptotic genes, *rpr* and *hid* in
1010 *stil*^{EY16156}*; P35 OE* and *stil*^{EY16156}*/CyO; P35 OE* ovaries. Expression levels were
1011 normalized to *αtub* with *rp49* as an internal control. Error bars indicate s.d. (*n*=3).
1012 (E) Immunofluorescence of Vasa (red) and DAPI (blue) in ovarioles from
1013 *stil*^{EY16156}*/CyO; rpr*^{87}/+, *stil*^{EY16156}*/CyO; rpr*^{87}*, stil*^{EY16156}*; rpr*^{87}/+, and *stil*^{EY16156}*;*
1014 *rpr*^{87}. Scale bar: 50 μm. (F) Quantification of the percentage of germline cell-
1015 containing ovarioles in 2-3-days old females. Genotypes of females and the
1016 number of germarium assessed are noted above each bar. Error bars represent
1017 standard deviation (s.d.). (G) Quantification of the percentage of developed
1018 ovarioles defined as ovarioles that contain at least two egg chambers beyond
1019 the germarium. Genotypes females and the number of germarium assessed
1020 are noted above each bar. Error bars represent standard deviation (s.d.). (H)
1021 Analysis of egg laying and hatching rate. Daily egg laying by three females
1022 indicated genotypes mated with three *y w* male and their hatching rate are
1023 shown (*n*=3). Error bar indicates s.d.

1024

1025 **Figure 4. Stil interacts with *rpr*-transcriptional control region to repress**
1026 **its expression**

1027 (A) Distribution of DamID peaks across entire genome categorized by genomic
1028 features including promoter (≤1, 1–2, and 2–3 kb), UTR, exon, intron, distal
1029 intergenic, and downstream. (B) The plot showing the $\log_2$ ratio of Dam-Stil

1030 peaks to Dam-alone control across the *rpr* genomic region. The blue bar on the
1031 bottom indicates the *rpr* gene body, and the arrow shows the direction of *rpr*
1032 transcription. Three independent biological replicates were performed for both
1033 Dam-Stil and Dam-alone and data were merged for visualization. (C) Schematic
1034 representation of the Stil full-length (Stil-FL), the truncated variants: Stil-NT (1st
1035 to 169th aa) and Stil-CT (169th to the end), and amino acid substitutions of the
1036 C2H2 zinc finger CCYC: Stil-AAYA. (D) *stil*^{EY16156} ovaries expressing Myc-
1037 tagged Stil variants corresponding to C in germline cells. Ovaries are
1038 immunostained with a germline marker, Vasa (red), and nuclear staining with
1039 DAPI (blue). Scale bar: 50 μm. (E) Quantification of the percentage of germline
1040 cell-containing ovarioles in 2-3 days-old females. Genotypes are indicated
1041 below the graph and the number of germarium assessed is noted above each
1042 bar. Error bars represent standard deviation (s.d.). (F) Quantification of the
1043 percentage of developed ovarioles defined as ovarioles that contain at least two
1044 egg chambers beyond the germarium. Genotypes are indicated below the
1045 graph and the number of germarium assessed is noted above each bar. Error
1046 bars indicate standard deviation (s.d.). (G) Schematic representation of *rpr*-
1047 GFP reporter containing the 5 kb upstream region and 5'-UTR of the *rpr* gene
1048 fused to GFP CDS. (H) Reporter assay in S2 cells followed by western blot
1049 analysis to detect GFP and α-Tubulin (αTub) as a loading control. Co-
1050 transfection of the *rpr*-GFP reporter and FLAG-tagged Stil variants were
1051 performed in S2 cells. The lower panel shows the signal ratio of GFP

1052 expression to αTub, normalized to that in cells transfected with the reporter
1053 alone. Error bars represent the standard deviation (s.d.) (n = 3).

1054

1055 **Figure 5. *stil* mutant germline stem cells resist apoptosis**

1056 (A) Fluorescent immunostaining with anti-Engrailed (red), anti-Vasa (green),
1057 and DAPI (blue) for terminal filaments of late 3rd instar larval (LL3) ovaries from
1058 the heterozygous control, *stil*^{EY16156}*/CyO* and *stil* mutant, *stil*^{EY16156}. Scale bar:
1059 50 μm. (B) Quantification of surviving germline cells in 3rd instar larval ovaries
1060 from *stil*^{EY16156}*/CyO* and *stil*^{EY16156}*.* (C) Immunostaining of Vasa (red) and DAPI
1061 (blue) in control, *Tkv.CA* (constitutive active Thickveins) *OE* (*NGT40; NosGal4-*
1062 *VP16>Tkv.CA*), and *bam* mutant (*bam*$^{\Delta 86}$) germaria (white dotted) in the control
1063 heterozygous (*stil*^{EY16156}*/CyO*) or *stil* mutant (*stil*^{EY16156}) background. Scale bar:
1064 20 μm. (D) Quantification germline cell-containing germaria per ovary in 2-3
1065 days-old females. Genotypes and the number of germarium assessed are
1066 indicated above each bar. Error bars represent standard deviation (s.d.). (E)
1067 Representative images of germaria (white dashed lines) showing TUNEL-
1068 positive apoptotic cells (green), Vasa (red), and DAPI (blue) in the control
1069 tumorous germaria (*stil*^{EY16156}*/CyO; Tkv.CA OE*) and tumorous germaria of *stil*
1070 mutant ovaries (*stil*^{EY16156}*; Tkv.CA OE*). White arrowheads indicate TUNEL-
1071 positive apoptotic cells. Scale bar: 20 μm. (F) Quantification of apoptosis in
1072 germaria from the control tumorous ovaries (*stil*^{EY16156}*/CyO; Tkv.CA OE*) and

1073 *stil* mutant ovaries (*stil*^{EY16156}*; Tkv.CA OE*). (G) MA plot of apoptosis-related
1074 genes showing the mean gene expression (CPM: counts per million) and fold
1075 change in *stil* mutant ovaries (*stil*^{EY16156}*; Tkv.CA OE*) compared to the control
1076 tumorous ovaries (*stil*^{EY16156}*/CyO; Tkv.CA OE*). Each dot represents an
1077 individual gene, with dot size inversely correlated with p-adj. The blue dots
1078 represent the downregulated genes with fold change<-2.0, and p-adj<0.01. (H)
1079 Quantitative RT-PCR analysis of *rpr* in the control tumorous ovaries
1080 (*stil*^{EY16156}*/CyO; Tkv.CA OE*) and *stil* mutant ovaries (*stil*^{EY16156}*; Tkv.CA OE*).
1081 Expression levels of an internal control, *rp49*, and *rpr* are normalized to that of
1082 *α-tub*. Error bars indicate s.d. (*n*=3).

1083

1084 **Figure 6. chromatin state changes in female germline cells during**
1085 **oogenesis**

1086 (A) ATAC-seq signal intensity (RPM-normalized) at the *rpr* locus in germline
1087 stem cells (GSCs: 2N and 4N) and nurse cells (NCs) at different ploidy levels
1088 (4C to 512C). The Y-axis is fixed at 0-30 PRM for all tracks. For 64C, 128C,
1089 256C, and 512C NCs, data from three biological replicates are averaged; all
1090 other samples are based on single replicates. (B) H3K9me3 ChIP-seq signal at
1091 the *rpr* locus in 4C GSCs and 4C NCs. (C) H3K27me3 ChIP-seq signal at
1092 the *rpr* locus in GSCs and stage 5 (st5) NCs. (D) Schematic model illustrating
1093 the *rpr* repression to inhibit the apoptotic cell death in undifferentiated germline

1094 cells (GSCs or GSC-like cells) and differentiated germline cells (nurse cells).

1095

1096 ## Supplementary Legends

1097 **Figure S1. *stil* function is indispensable in female germline cells not**

1098 **male germline cells**

1099 (A) Immunostaining of ovaries from *y w*, *stil*^{3}*/CyO*, *stil*^{3}*/Df*, and *stil*^{3}*/stil*^{EY16156}

1100 with antibody against Vasa (red) with DAPI (blue). Scale bar: 50 μm. (B)

1101 Quantification of the percentage of germline cell-containing ovarioles in 2-3

1102 days old females. (C) Immunostaining of the apical end of testes from

1103 *stil*^{EY16156}*/CyO* and *stil*^{EY16156} with anti-Vasa antibody (red) and DAPI (blue) (top

1104 panels). Seminal vesicles (SV) harboring sperms are also stained with DAPI

1105 (blue) (bottom panels). Asterisk denotes the apex of testis. Scale bar: 50μm

1106 (apical end of testes, top) and 20 μm (SV, bottom). (D) The numbers of egg

1107 laying and hatching rate. Daily egg laying by three *y w* females mated with three

1108 males of the indicated genotypes are shown (*n*=3). The number of ovarioles

1109 assessed is noted above each bar. Error bar indicates s.d.

1110

1111 **Figure S2. Germline knockdown of *stil*, but not somatic knockdown,**

1112 **specifically disrupts egg development**

1113 (A) Analysis of egg laying and hatching rates. The number of laid eggs and their

1114 hatching rates are measured daily for three females of the indicated genotypes:

1115 control, *stil*-germline knockdown (*stil*-GLKD) driven by *NGT40; NosGal4-VP16*,

1116 and *stil*-somatic knockdown (*stil*-STKD) driven by *tj-Gal4*, each mated with

1117 three *y w* males (*n* = 3). Error bars indicate standard deviation (s.d.). (B) RT-

1118 PCR analysis of *sxl* and the control, *α-tub* transcripts in ovaries and testes from
1119 control and *stil*-GLKD flies, respectively.

1120

1121 **Figure S3. Egg development is disrupted at the mid-stage of oogenesis**
1122 **in *stil* mutants rescued by P35 or DIAP1**

1123 Immunostaining of ovarioles from *y w*, *stil*^{EY16156}/*CyO; P35 OE* (*NGT40;*
1124 *NosGal4-VP16> P35*), *stil*^{EY16156}*; P35 OE* and *stil*^{EY16156}*; DIAP1 OE* (*NGT40;*
1125 *NosGal4-VP16> DIAP1*) flies with antibody against Vasa (red) and DAPI (blue).
1126 The enlarged image highlights a degenerated egg chamber at the mid-stage of
1127 oogenesis in *stil*^{EY16156}*; P35 OE*. Scale bar: 50 μm.

1128

1129 **Figure S4. BED-type zinc finger of Stil and transcriptome analysis of**
1130 **germline-rescued *stil* mutant ovaries**

1131 (A) A schematic presentation of Stil protein, highlighting the BED-type zinc
1132 finger (BED, green) and the nuclear localization signal (NLS, blue). A multiple
1133 sequence alignment of Stil with three other proteins containing BED-type zinc
1134 finger motif is shown. The BED-type zinc finger motif consists of two cysteine
1135 and histidine residues (red) and aromatic residues (yellow) in the N-terminal
1136 region. (B) Transcriptome analysis of germline-rescued *stil* mutant ovaries
1137 expressing P35. Differential expressed genes (DEGs) are obtained with
1138 DEseq2. Volcano plot displays the adjusted *p*-value (*p*-adj) versus log2-fold

1139 change (log2FC) of expression level in *stil*^{EY16156}*; P35 OE* compared to that in
1140 *stil*^{EY16156}*/CyO; P35 OE*. Significantly upregulated genes (log2FC > 1, *p*-adj <
1141 0.01) and downregulated genes (log2FC < -1, *p*-adj < 0.01) are highlighted in
1142 red and blue, respectively, while non-DEGs are shown in black.

1143

1144 **Figure S5. *rpr*, but not *hid*, plays a central role in *stil*-deficient female**
1145 **germline cell death**

1146 (A-C) Quantitative RT-PCR are performed on ovaries from germline-rescued
1147 *stil* mutants, as well as ovaries and testes with germline-specific *stil* knockdown
1148 using distinct drivers. Expression levels are normalized to *αtub* with *rp49*
1149 serving as an internal control. (A) Early-stage ovaries are isolated by dissecting
1150 stage 4–5 oocytes from *stil*^{EY16156}*/CyO; P35 OE* and *stil*^{EY16156}*; P35 OE* flies (B)
1151 *stil* knockdown in female germline cells is achieved using *NGT40-Gal4;*
1152 *NosGal4-VP16*, *Bam-Gal4*, and *matα-tub-Gal4* drivers. (C) *stil* knockdown in
1153 male germline cells is achieved using *NGT40-Gal4; NosGal4-VP16* and *Bam-*
1154 *Gal4* drivers. Error bars represent standard deviation (s.d.). (D) Immunostaining
1155 of *stil*^{EY16156}*; hid*^{05014}*/+* and *stil*^{EY16156}*; hid*^{05014}*/Df(3L)X14* ovaries with antibody
1156 against Vasa (red) with DAPI (blue). Scale bar: 50 μm. (E) Quantification of the
1157 percentage of germline cell-containing ovarioles in 2-3-days old females. The
1158 number of ovarioles assessed is noted above each bar.

1159

1160 **Figure S6. Stil variants localization and control validation in S2 reporter**

1161 **assay**

1162 (A) Immunofluorescence images showing Myc-tagged Stil variants (green) and

1163 DNA (DAPI, blue) in stage 3~4 egg chambers of the ovaries. Insets show

1164 enlarged views of nurse cell nuclei. Scale bar: 50 μm (egg chamber) and 20 μm

1165 (nurse cell nuclei). (B) Immunostaining of S2 cells expressing FLAG-tagged Stil

1166 variants with an anti-FLAG (green) antibody and DAPI (blue). (C) Schematic

1167 representation of the *ubiP*-GFP reporter construct, in which the 2,173 bp

1168 upstream region and 5'-UTR of the *ubi-p63E* gene is fused to GFP. (D) Reporter

1169 assay in S2 cells followed by western blot analysis to detect GFP expression.

1170 Co-transfection of the *ubiP*-GFP reporter and FLAG-tagged Stil-FL were

1171 performed in S2 cells. An arrowhead indicates Stil-FL protein. *α*-Tubulin (αTub)

1172 is used as a loading control. The lower panel quantifies the GFP/αTub signal

1173 ratio, normalized to that in S2 cells transfected with the reporter alone. Error

1174 bars indicate standard deviation (s.d.) (n = 3).

Figure 1

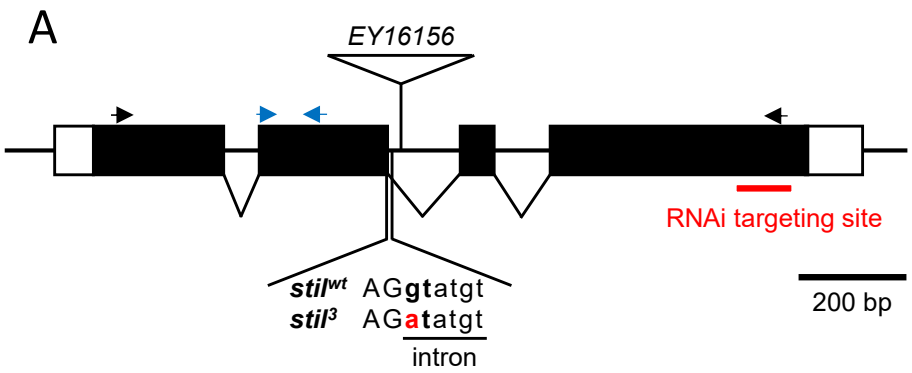
A
EY16156
RNAi targeting site
stil^wt AGgtatgt
stil^3 AGatatgt
intron
200 bp

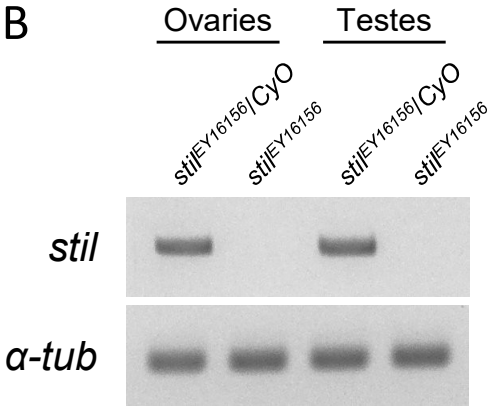
B
Ovaries
Testes
stil^EY16156/CyO
stil^EY16156
stil^EY16156/CyO
stil^EY16156
stil
α-tub

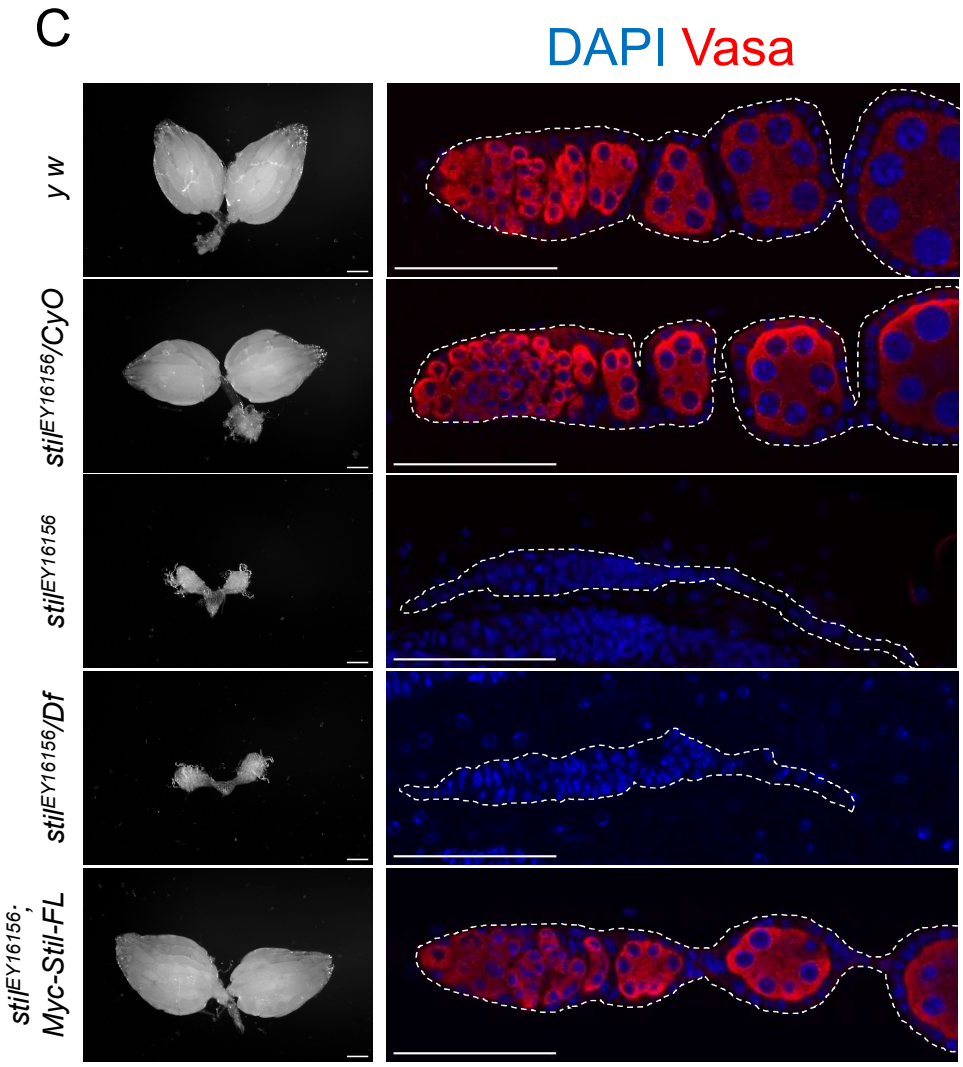
C
DAPI Vasa
y w
stil^EY16156/CyO
stil^EY16156
stil^EY16156/Df
stil^EY16156; Myc-Stil-FL

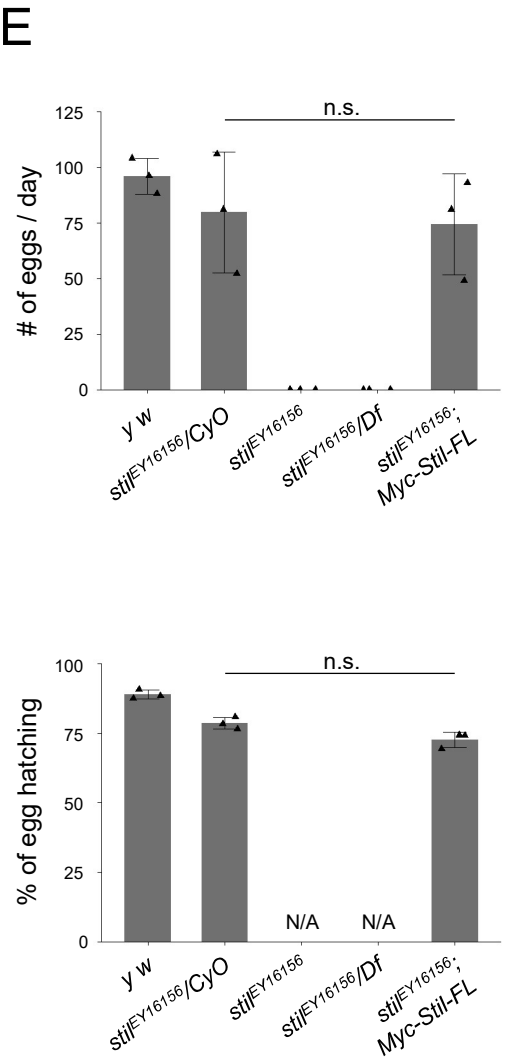
E
n.s.
# of eggs / day
125
100
75
50
25
0
y w
stil^EY16156/CyO
stil^EY16156
stil^EY16156/Df
stil^EY16156; Myc-Stil-FL
n.s.
% of egg hatching
100
75
50
25
0
N/A
N/A

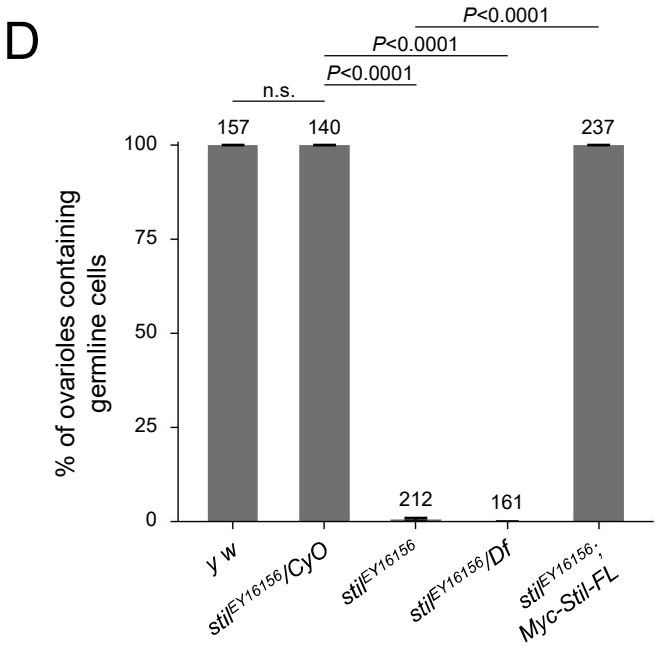
D
P<0.0001
P<0.0001
P<0.0001
n.s.
% of ovarioles containing germline cells
100
75
50
25
0
157
140
212
161
237
y w
stil^EY16156/CyO
stil^EY16156
stil^EY16156/Df
stil^EY16156; Myc-Stil-FL

Figure 2

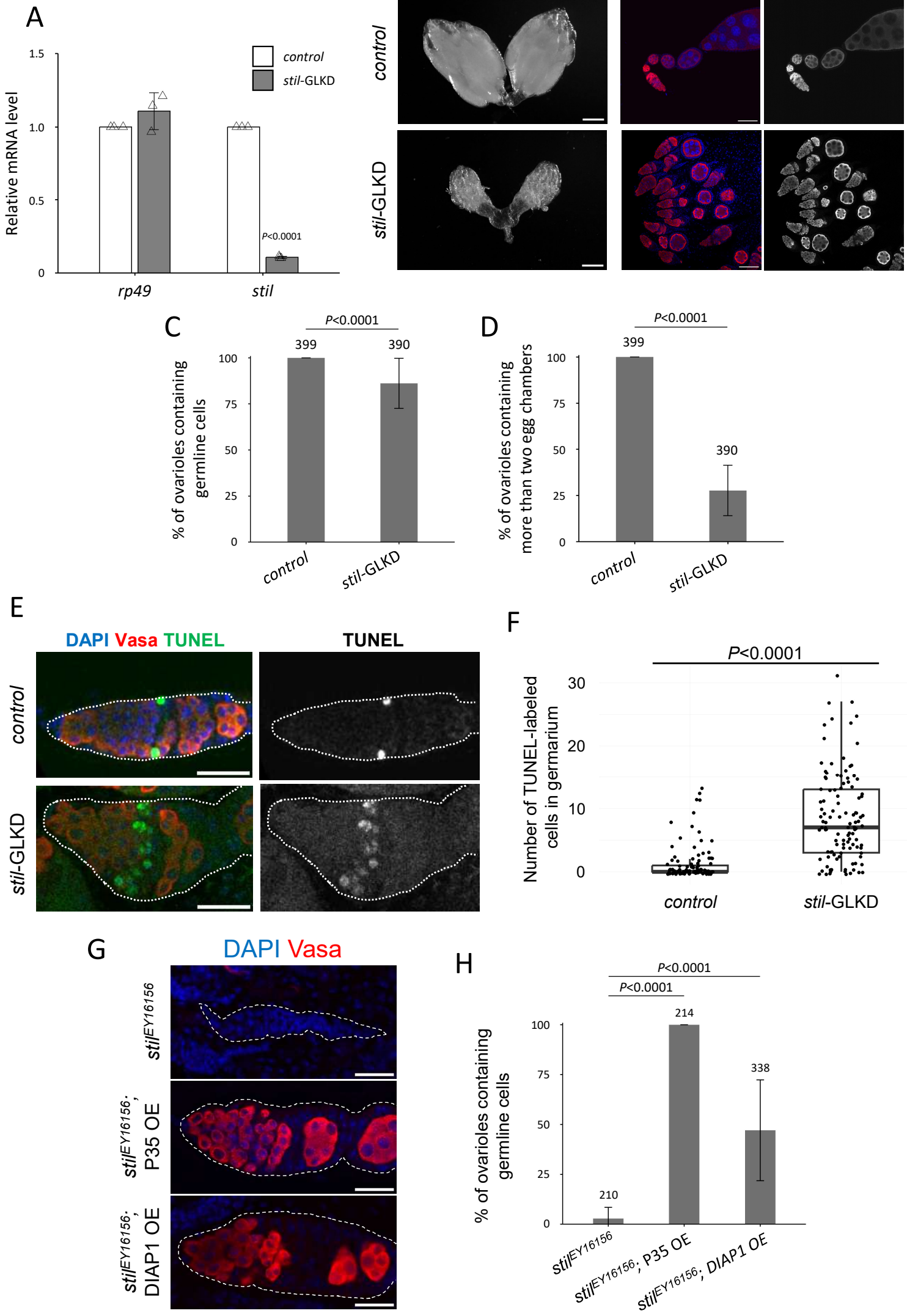
A
Relative mRNA level
1.5
1.0
0.5
0
control
stil-GLKD
P<0.0001
rp49
stil
B
DAPI Vasa
Vasa
control
stil-GLKD
C
P<0.0001
399
390
% of ovarioles containing germline cells
100
75
50
25
0
control
stil-GLKD
D
P<0.0001
399
390
% of ovarioles containing more than two egg chambers
100
75
50
25
0
control
stil-GLKD
E
DAPI Vasa TUNEL
TUNEL
control
stil-GLKD
F
P<0.0001
Number of TUNEL-labeled cells in germarium
30
20
10
0
control
stil-GLKD
G
DAPI Vasa
stilEY16156
stilEY16156; P35 OE
stilEY16156; DIAP1 OE
H
P<0.0001
P<0.0001
214
338
210
% of ovarioles containing germline cells
100
75
50
25
0
stilEY16156
stilEY16156; P35 OE
stilEY16156; DIAP1 OE

Figure 3

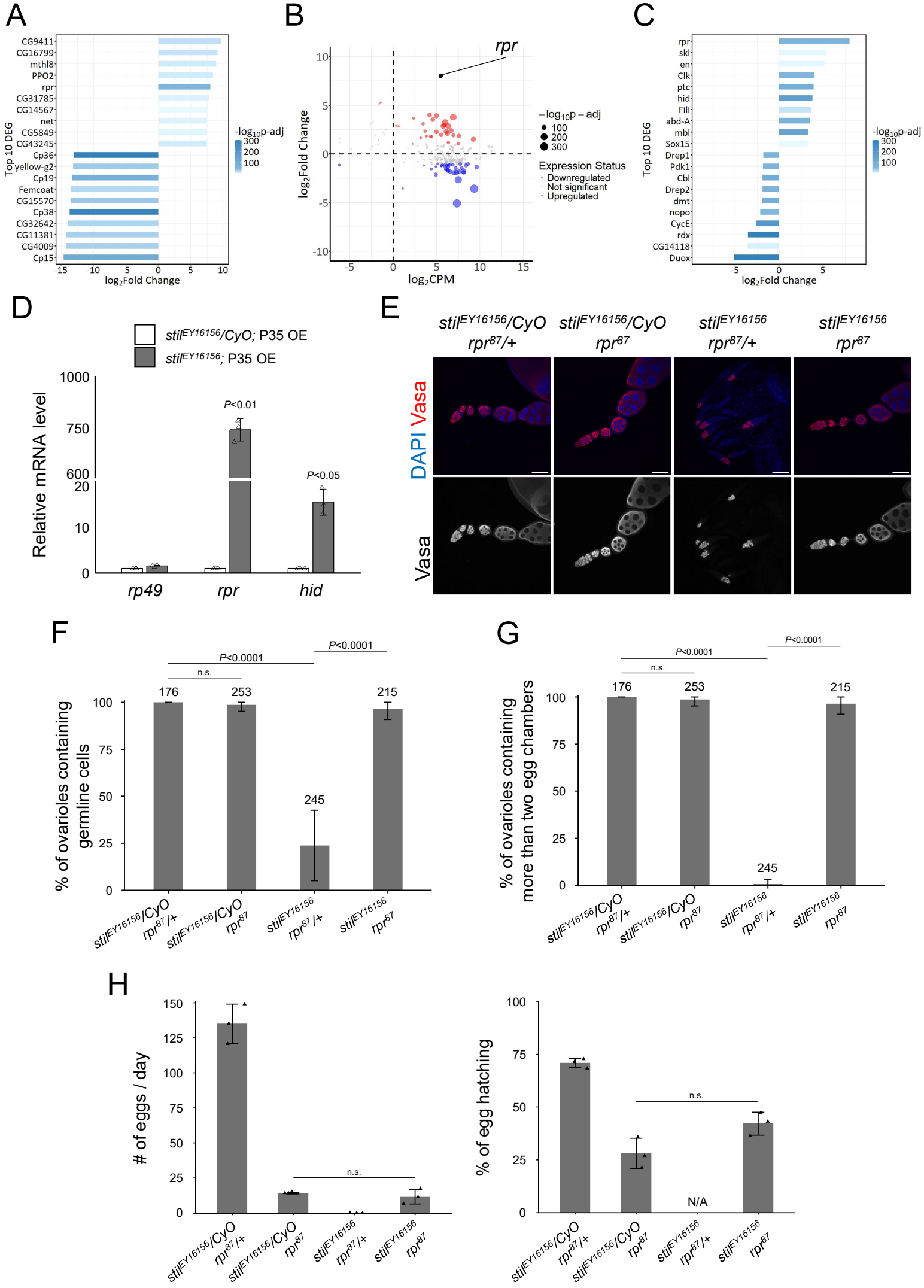
A
CG9411
CG16799
mthl8
PPO2
rpr
CG31785
CG14567
net
CG5849
CG43245
Cp36
yellow-g2
Cp19
Femcoat
CG15570
Cp38
CG32642
CG11381
CG4009
Cp15
Top 10 DEG
log2Fold Change
-log10p-adj
300
200
100
B
rpr
log2Fold Change
log2CPM
−log10p − adj
100
200
300
Expression Status
Downregulated
Not significant
Upregulated
C
rpr
skl
en
Clk
ptc
hid
Fili
abd-A
mbl
Sox15
Drep1
Pdk1
Cbl
Drep2
dmt
nopo
CycE
rdx
CG14118
Duox
Top 10 DEG
log2Fold Change
-log10p-adj
300
200
100
D
stilEY16156/CyO; P35 OE
stilEY16156; P35 OE
Relative mRNA level
P<0.01
P<0.05
rp49
rpr
hid
E
stilEY16156/CyO rpr87/+
stilEY16156/CyO rpr87
stilEY16156 rpr87/+
stilEY16156 rpr87
DAPI Vasa
Vasa
F
P<0.0001
P<0.0001
n.s.
% of ovarioles containing germline cells
176
253
245
215
stilEY16156/CyO rpr87/+
stilEY16156/CyO rpr87
stilEY16156 rpr87/+
stilEY16156 rpr87
G
P<0.0001
P<0.0001
n.s.
% of ovarioles containing more than two egg chambers
176
253
245
215
stilEY16156/CyO rpr87/+
stilEY16156/CyO rpr87
stilEY16156 rpr87/+
stilEY16156 rpr87
H
# of eggs / day
n.s.
stilEY16156/CyO rpr87/+
stilEY16156/CyO rpr87
stilEY16156 rpr87/+
stilEY16156 rpr87
% of egg hatching
n.s.
N/A
stilEY16156/CyO rpr87/+
stilEY16156/CyO rpr87
stilEY16156 rpr87/+
stilEY16156 rpr87

Figure 4

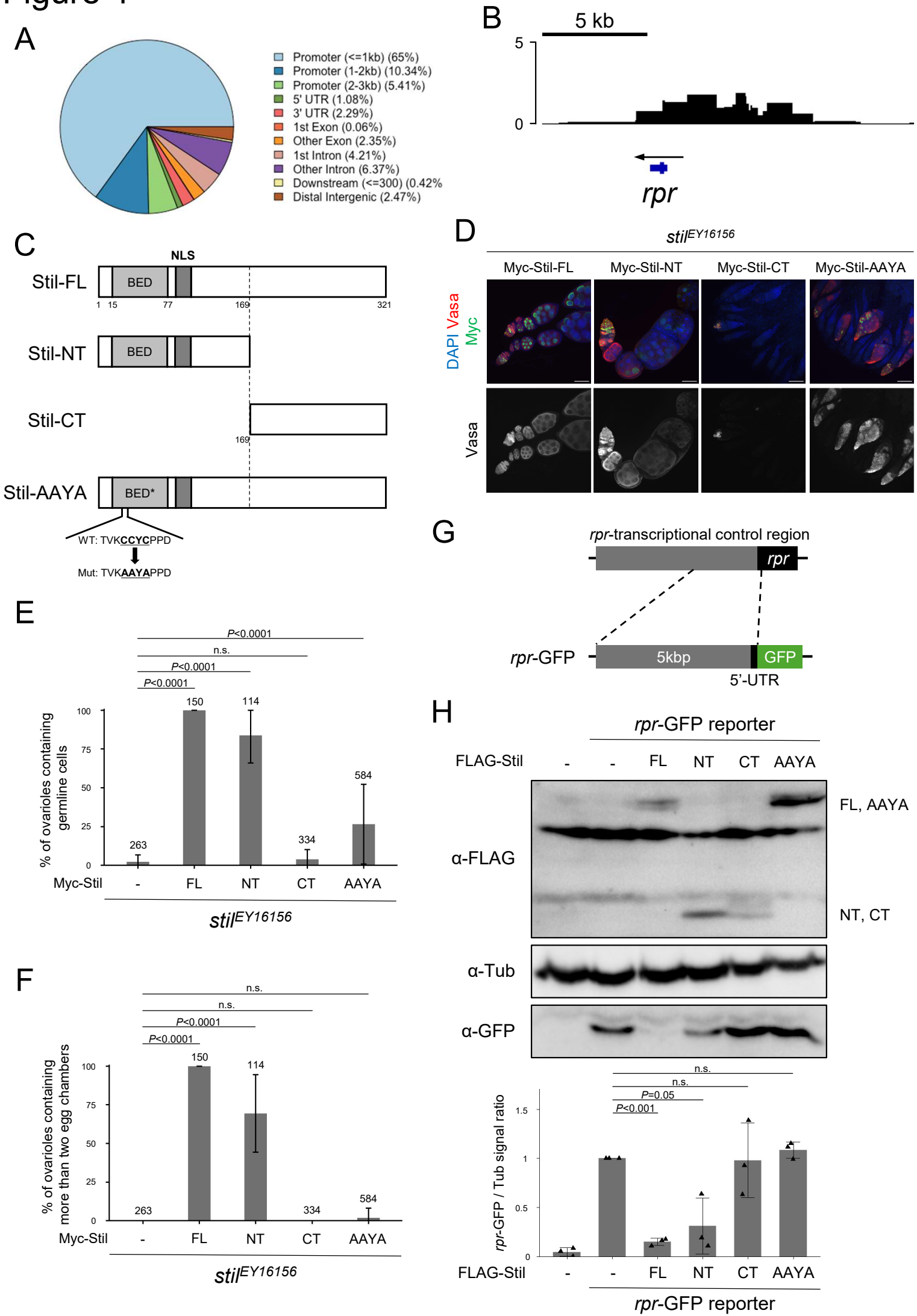
A
Promoter (<=1kb) (65%)
Promoter (1-2kb) (10.34%)
Promoter (2-3kb) (5.41%)
5' UTR (1.08%)
3' UTR (2.29%)
1st Exon (0.06%)
Other Exon (2.35%)
1st Intron (4.21%)
Other Intron (6.37%)
Downstream (<=300) (0.42%
Distal Intergenic (2.47%)
B
5 kb
5
0
rpr
C
NLS
Stil-FL
BED
1 15 77 169 321
Stil-NT
BED
Stil-CT
169
Stil-AAYA
BED*
WT: TVKCCYCPPD
Mut: TVKAAYAPPD
D
stilEY16156
Myc-Stil-FL
Myc-Stil-NT
Myc-Stil-CT
Myc-Stil-AAYA
DAPI Vasa Myc
Vasa
E
P<0.0001
n.s.
P<0.0001
P<0.0001
% of ovarioles containing germline cells
100
75
50
25
0
263
150
114
334
584
Myc-Stil
-
FL
NT
CT
AAYA
stilEY16156
F
n.s.
n.s.
P<0.0001
P<0.0001
% of ovarioles containing more than two egg chambers
100
75
50
25
0
263
150
114
334
584
Myc-Stil
-
FL
NT
CT
AAYA
stilEY16156
G
rpr-transcriptional control region
rpr
rpr-GFP
5kbp
GFP
5'-UTR
H
rpr-GFP reporter
FLAG-Stil
-
-
FL
NT
CT
AAYA
FL, AAYA
α-FLAG
NT, CT
α-Tub
α-GFP
n.s.
n.s.
P=0.05
P<0.001
rpr-GFP / Tub signal ratio
1.5
1
0.5
0
FLAG-Stil
-
-
FL
NT
CT
AAYA
rpr-GFP reporter

Figure 5

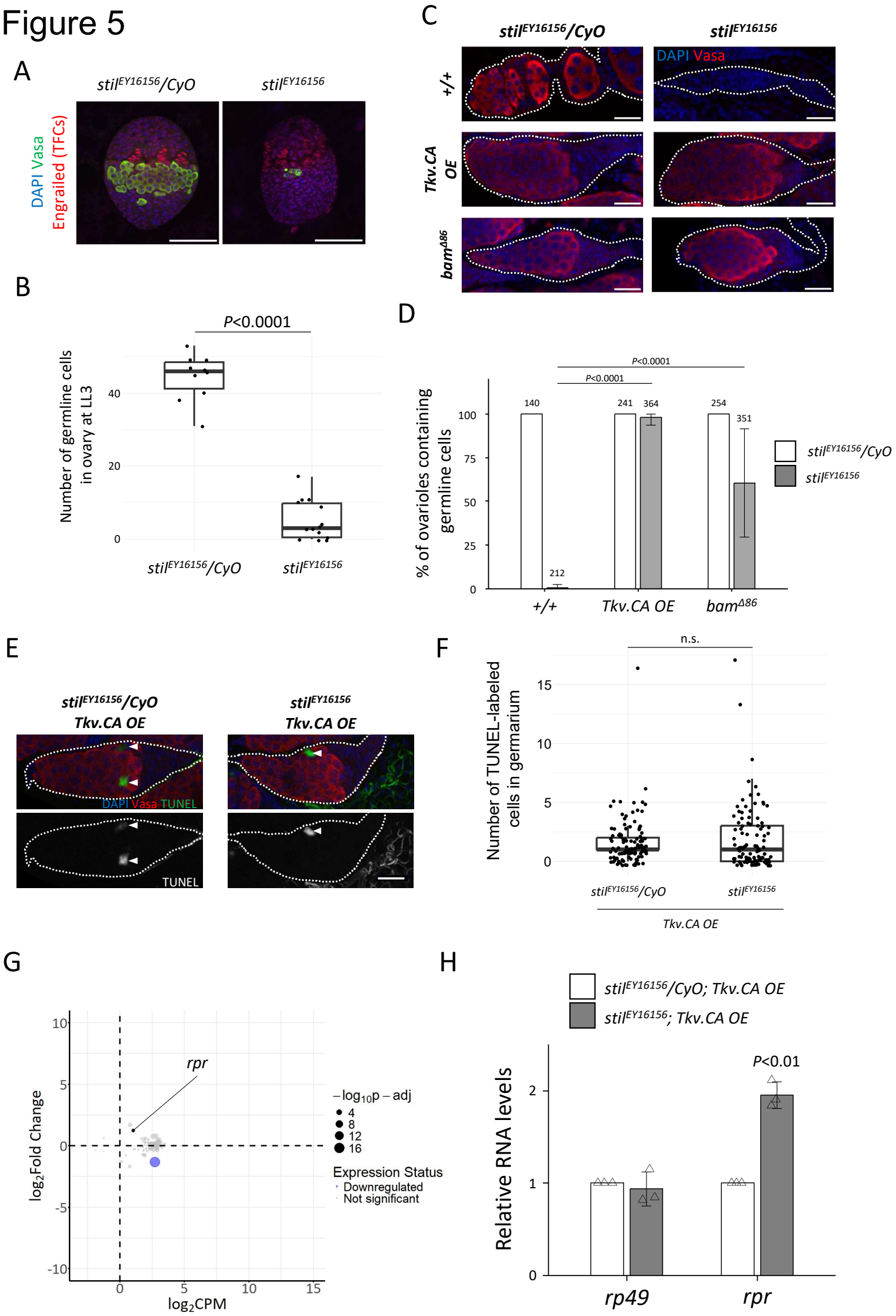
A
stilEY16156/CyO
stilEY16156
DAPI Vasa
Engrailed (TFCs)
B
P<0.0001
Number of germline cells in ovary at LL3
40
20
0
stilEY16156/CyO
stilEY16156
C
stilEY16156/CyO
stilEY16156
+/+
Tkv.CA OE
bamΔ86
DAPI Vasa
D
P<0.0001
P<0.0001
% of ovarioles containing germline cells
100
75
50
25
0
140
212
241
364
254
351
+/+
Tkv.CA OE
bamΔ86
stilEY16156/CyO
stilEY16156
E
stilEY16156/CyO Tkv.CA OE
stilEY16156 Tkv.CA OE
DAPI Vasa TUNEL
TUNEL
F
n.s.
Number of TUNEL-labeled cells in germarium
15
10
5
0
stilEY16156/CyO
stilEY16156
Tkv.CA OE
G
rpr
log2Fold Change
10
5
0
-5
-10
0
5
10
15
log2CPM
−log10p−adj
4
8
12
16
Expression Status
Downregulated
Not significant
H
stilEY16156/CyO; Tkv.CA OE
stilEY16156; Tkv.CA OE
P<0.01
Relative RNA levels
2
1
0
rp49
rpr

Figure 6

A

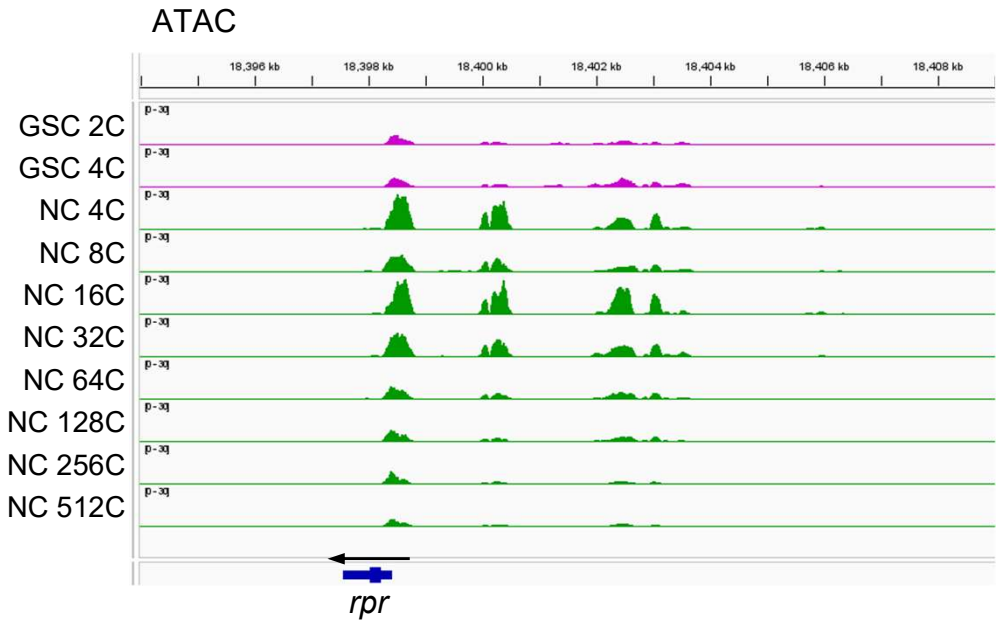

B

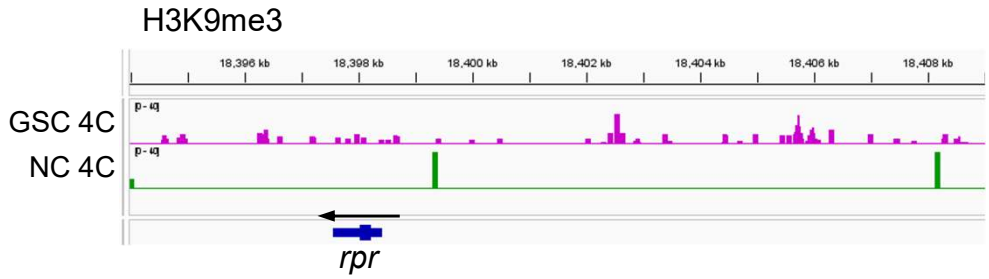

C

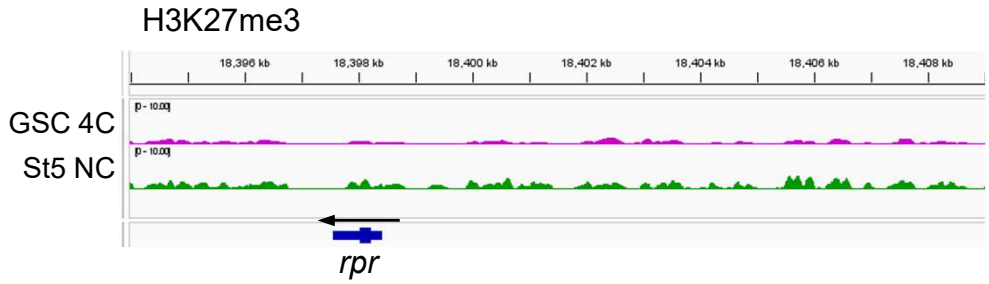
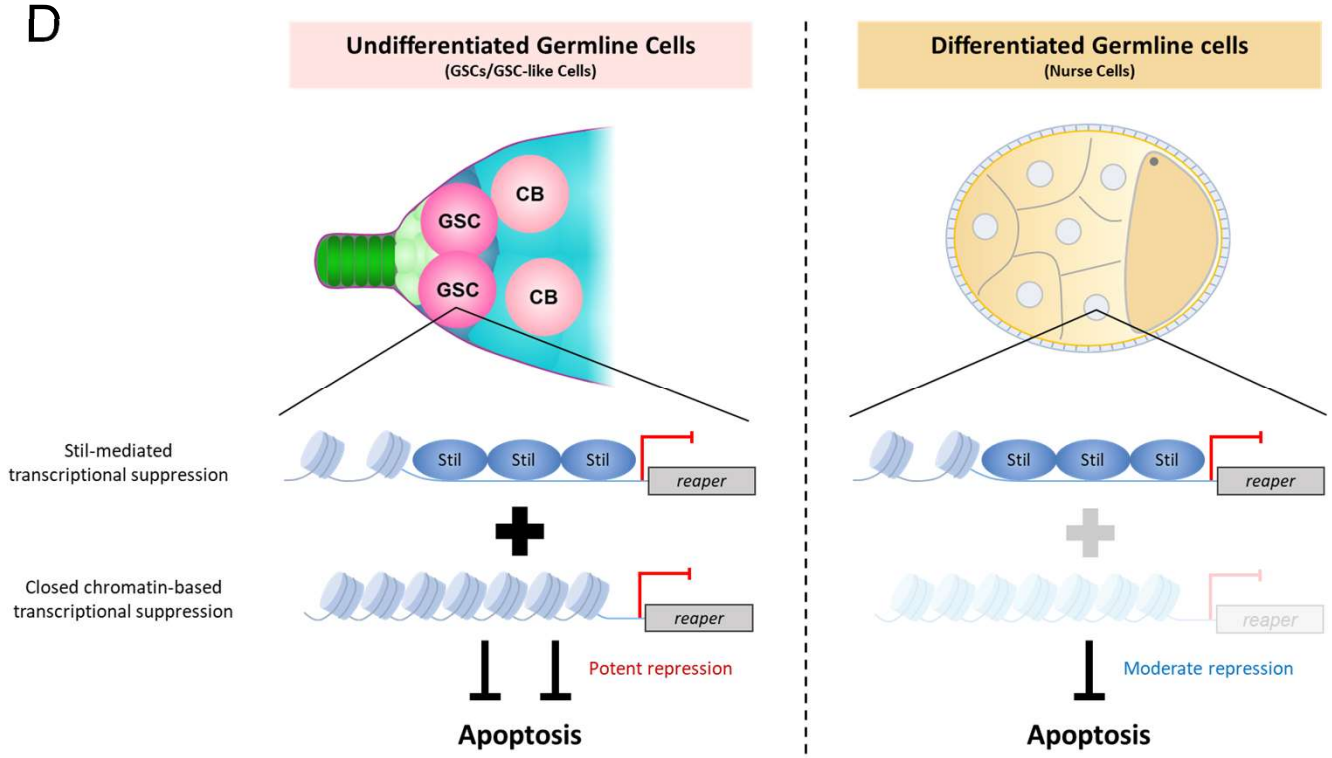
D